

Predicting COVID-19 hospitalisation using a mixture of Bayesian predictive syntheses

Genya Kobayashi^{1*}, Shonosuke Sugasawa², Yuki Kawakubo³,
Dongu Han⁴ and Taeryon Choi⁴

¹School of Commerce, Meiji University, Japan

²Faculty of Economics, Keio University, Japan

³Graduate School of Social Sciences, Chiba University, Japan

⁴Department of Statistics, Korea University, Korea

Abstract

This paper proposes a novel methodology called the mixture of Bayesian predictive syntheses (MBPS) for multiple time series count data for the challenging task of predicting the numbers of COVID-19 inpatients and isolated cases in Japan and Korea at the subnational-level. MBPS combines a set of predictive models and partitions the multiple time series into clusters based on their contribution to predicting the outcome. In this way, MBPS leverages the shared information within each cluster and is suitable for predicting COVID-19 inpatients since the data exhibit similar dynamics over multiple areas. Also, MBPS avoids using a multivariate count model, which is generally cumbersome to develop and implement. Our Japanese and Korean data analyses demonstrate that the proposed MBPS methodology has improved predictive accuracy and uncertainty quantification.

Key words: clustering; count data; dynamic factor model; finite mixture model; Markov chain Monte Carlo; Pólya-gamma augmentation; state space model

1 Introduction

The outbreak of COVID-19 caused tremendous social and economic disruption all over the world. During the pandemic that the modern world had not experienced, there were

*Author of correspondence: gkobayashi@meiji.ac.jp

explosions in the various academic fields to investigate and predict the various aspects of the pandemic and its influence.

In Japan, COVID-19 was classified as Category II Infectious Diseases under the Infectious Diseases Control Law until 7 May 2023. During the pandemic, infected individuals were isolated, and patients with severe conditions received treatment in designated beds. The number of designated beds is limited and varied across the prefectures of Japan. In the fall and winter of 2021, when the Omicron variant (BA-5 virus) spread dramatically, there was a deep concern about the shortage of designated beds for COVID-19 patients. In Korea, COVID-19 was classified as a first-grade infectious disease by the Korea Centers for Disease Control and Prevention (KCDC) until 24 April 2022. As in Japan, infected individuals underwent isolation or hospitalisation depending on the severity of the condition. The emergence of the Omicron variant also led to a significant increase in isolated individuals. These backgrounds highlight the need for quick responses by national and local governments to rapid changes in healthcare demand and for efficient resource allocation, which are based on accurate patient prediction, desirably, at the subnational level.

Hence, the aim of this paper is to provide a novel statistical method that performs reasonably well in predicting the numbers of inpatients and isolated cases in Japan and Korea at the subnational level. From the early stage of the pandemic, many studies tried to predict its course or extract the trend using existing and new methods (see Rahimi et al., 2023). However, due to the very complex and unexpected dynamics of the pandemic caused by the rise of new variants, government interventions, and various formal and informal prevention measures, it is not possible for a single model to consistently outperform others. Therefore, instead of implementing a single overly complex model to predict the course of the pandemic, combining predictions from a set of relatively simple predictive models would be more fruitful, as demonstrated by Paireau et al. (2022) and Chowell et al. (2022), which performed an ensemble prediction for several indicators of the country-level healthcare demand in France and the United States, respectively.

Therefore, we develop a novel statistical method that combines multiple predictive models, specifically focusing on the emerging approach called Bayesian predictive synthesis (BPS) proposed by McAlinn and West (2019). BPS is a coherent Bayesian framework for synthesising multiple predictive models, called agent models, based on the agent opinion

analysis of, for example, Genest and Schervish (1985) and West and Crosse (1992). The recent studies on BPS include McAlinn et al. (2020) for multivariate time series, McAlinn (2021) for mixed-frequency time series, Cabel et al. (2023) for spatial data and Sugawara et al. (2023) for the meta-inference of heterogeneous treatment effects. Notably, Cabel et al. (2023) showed that their BPS methodology is exact minimax. Tallman and West (2023) considered BPS in the general Bayes setting. Johnson and West (2023) proposed several ways to construct synthesis weights that depend on the outcomes. Chernis (2022) considered the situation where an analyst has many agent models to be combined and proposed the shrinkage approach to suppress the contribution of redundant models and the factor approach to reduce the number of latent variables. See also Aastveit et al. (2019) for a review of other forecast combination methods and references therein.

Since the numbers of inpatients and isolated cases in Japan and Korea constitute time series count data over multiple areas of the countries, we propose a novel BPS methodology for multiple time series count data called the mixture of Bayesian predictive syntheses (MBPS). In our analysis, we have the count time series for 47 prefectures of Japan and 17 Metropolitan Autonomous Governments (MAGs) of Korea. Instead of treating multiple count time series using multivariate models, the proposed MBPS partitions them into clusters based on the finite mixture of BPS since the specification and implementation of multivariate count time series models are generally cumbersome (Davis et al., 2021; Fokianos, 2021; West, 2020). Introducing a clustering structure is motivated by the observation that a group of time series in our data exhibits similar dynamics. In MBPS, the agent models are assigned the same synthesis weights for the time series in the cluster. In this way, MBPS can leverage the shared information across time series based on the similarity in the contribution of the agent models to predicting the outcomes. Our MBPS is similar to the time series clustering methods based on the parametric models reviewed in Frühwirth-Schnatter (2011) and the nonparametric Bayesian approach of Nieto-Barajas and Contreras-Cristán (2014) and Lin et al. (2019), in the sense that they have cluster-specific parameters and latent variables. Note that the existing BPS approaches do not consider such a clustering structure. The clustering structure of MBPS can reduce the number of parameters and model complexity compared to a fully multivariate count model. Each agent model fed into MBPS can be univariate, and the individual univariate pre-

dictions are combined through the mixture of synthesised predictive distributions. It is appealing because there is an abundance of univariate count models (Davis et al., 2016, 2021; Fokianos, 2021). Thus, one can easily choose and fit a set of univariate models used in MBPS.

The remainder of this paper is organised as follows. Section 2 introduces the data on the number of COVID-19 inpatients in the prefectures of Japan and number of isolated cases in the MAGs of Korea. Section 3 first briefly describes BPS. Then, we propose the novel BPS for time series count data and introduce MBPS for multiple time series count data and its variants. Using MBPS, Section 4 analyses the COVID-19-related data on the numbers of inpatients in Japan and isolated cases in Korea, where the proposed method demonstrates improved predictive accuracy and uncertainty quantification. Finally, Section 5 provides some conclusion and discussion.

2 Data

We obtained the weekly numbers of COVID-19 inpatients in the 47 prefectures of Japan from the Ministry of Health, Labour and Welfare of Japan (<https://www.mhlw.go.jp>). The data are publicly available. The total data period is from 7 May 2020 to 23 November 2022 (134 weeks). Figure 1 shows the time series plots between 21 April 2021 and 23 November 2022. In the figure, the prefectures are grouped arbitrarily into each panel based on the average number of inpatients over the data period for visibility. In the figure, the dynamics among the time series are very similar, with surges as the new variants prevailed and drops as the immunity to them was gained.

In Korea, KCDC provides the open data via the public data portal (<https://www.data.go.kr>). The dataset consists of the number of daily isolated cases of COVID-19 from the 17 MAG, spanning from 1 August 2020 to 30 November 2021, totalling 487 days. We could not access additional data beyond this period as the Korean government ceased publishing the number of daily isolated cases starting in December 2021. Figure 2 presents the time series plot of the Korean data over the estimation and prediction periods where MAGs are grouped based on the averages of the isolated people over the data period. As in the Japanese data, the data exhibit similar dynamics among the series.

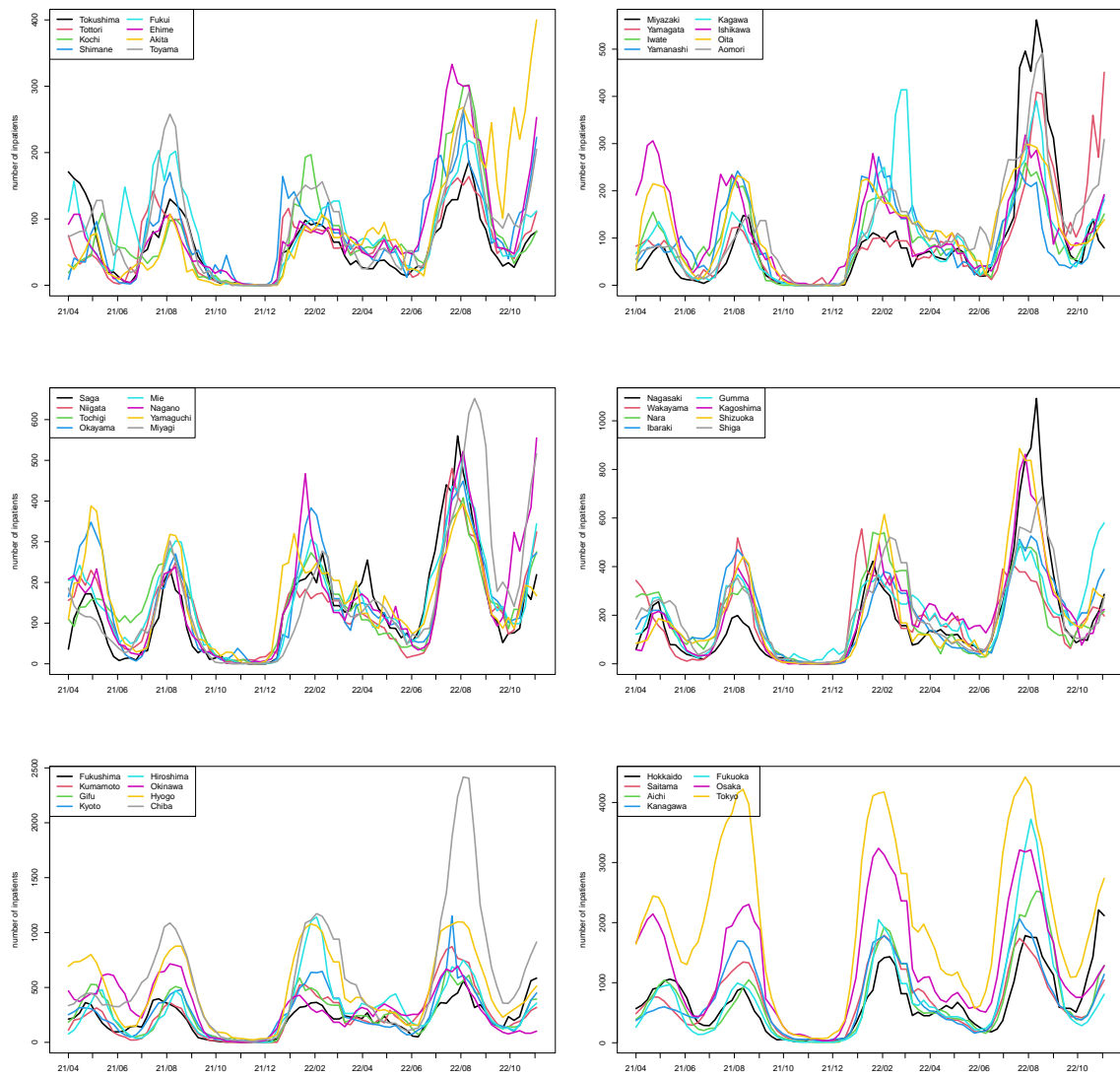


Figure 1: Time series plots of the numbers of inpatients in Japan. The prefectures are grouped based on the means of the inpatients over the data period.

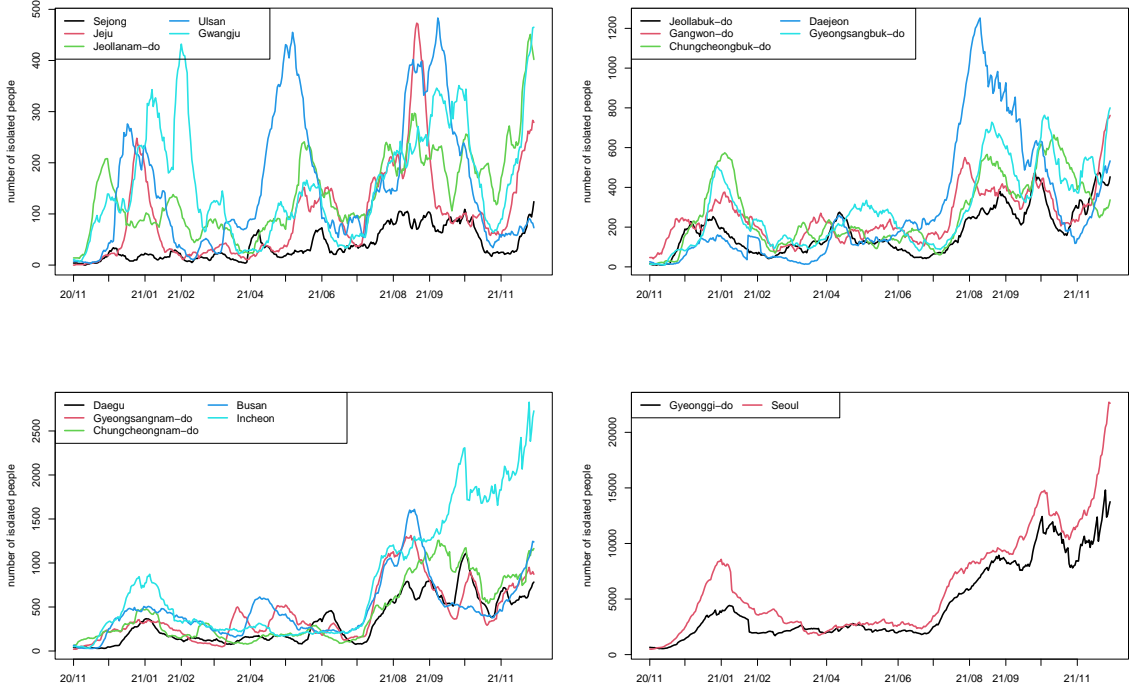


Figure 2: Time series plots of the number of isolated people in Korea. The MAGs are grouped based on the averages of the isolated people over the data period.

3 Method

3.1 Bayesian predictive synthesis

Consider a univariate time series data denoted by y_t for $t = 1, 2, \dots$. An analyst elicits J agent models with the predictive density denoted by $h_{tj}(f_{tj})$ for $j = 1, \dots, J$. Then to predict y_t at the time $t-1$, the collection of J predictive densities forms an information set denoted by $\mathcal{H}_t = (h_{t1}(y_t), \dots, h_{tJ}(y_t))$. The available information is $\{y_{1:t-1}, \mathcal{H}_{1:t}\}$. The Bayesian predictive synthesis considers the following synthesised predictive distribution (McAlinn and West, 2019):

$$p(y_t | \Phi_t, y_{1:t-1}, \mathcal{H}_{1:t}) \equiv p(y_t | \Phi_t, \mathcal{H}_t) = \int \alpha(y_t | \mathbf{f}_t, \Phi_t) \left[\prod_{j=1}^J h_{tj}(f_{tj}) \right] d\mathbf{f}_t,$$

where $\alpha(y_t | \mathbf{f}_t, \Phi_t)$ denotes the synthesis function which controls how to combine J predictions from the agent models, Φ_t is the collection of parameters of the synthesis function,

$\mathbf{f}_t = (f_{t1}, \dots, f_{tJ})'$ denotes the draw from the predictive densities that are regarded as the latent factors. The design of the synthesis function and prior structure of the synthesis weights are left to the analyst's discretion. Thus, the model can vary depending on the purpose of the analysis and the type and potential dependence structure of the data.

When y_t is supported on the real line, McAlinn and West (2019) proposed the use of the normal probability density $\alpha(y_t|\mathbf{f}_t, \Phi_t) = \phi(y_t; \mu_t, \sigma_t^2)$ as the synthesis function, where $\phi(\cdot; \mu, \sigma^2)$ denotes the probability density function of $N(\mu, \sigma^2)$. Introducing the synthesis weights for the J agent models, the mean μ_t is modelled as $\mu_t = \boldsymbol{\theta}_t' \mathbf{F}_t$ where $\boldsymbol{\theta}_t = (\theta_{t0}, \theta_{t1}, \dots, \theta_{tJ})'$ is the $(J+1) \times 1$ vector of the synthesis weights and $\mathbf{F}_t = (1, \mathbf{f}_t)'$. The predictive distribution of j th agent model for y_t may be typically given by the normal distribution, $h_{tj}(y_t) = \phi(y_t; m_{tj}, s_{tj}^2)$ for $j = 1, \dots, J$. The mean and variance of this normal distribution are obtained exactly or by analytic or numerical approximation based on each agent. Since the latent factor f_{tj} is a draw from h_{tj} in BPS, the synthesised predictive model for the continuous y_t can be written in the form of a normal factor model: $y_t|\boldsymbol{\theta}_t' \mathbf{F}_t, \sigma_t^2 \sim N(\boldsymbol{\theta}_t' \mathbf{F}_t, \sigma_t^2)$, $f_{tj} \sim N(m_{tj}, s_{tj}^2)$, $j = 1, \dots, J$, for $t = 1, 2, \dots$. In this case, $\Phi_t = (\boldsymbol{\theta}_t, \sigma_t^2)$. Furthermore, an appropriate model for $\boldsymbol{\theta}_t$ can be specified; see Section 3.2. The synthesis weights $\boldsymbol{\theta}_t$ are not constrained to be in the J -simplex and allow negative weights. Thus, when θ_{tj} for some j is close to zero, the corresponding agent model does not contribute to predicting y_t . The intercept θ_{t0} captures the remaining part of predicting y_t and can be interpreted as the inadequacy of the predictive performance of the agent models.

When y_t is the univariate count data, we propose to use the Poisson probability mass function for $\alpha(y_t|\mathbf{f}_t, \Phi_t)$ with $\Phi_t = \boldsymbol{\theta}_t$. Therefore, conditionally on the latent factors \mathbf{f}_t and synthesis weights $\boldsymbol{\theta}_t$, we have

$$y_t|\boldsymbol{\theta}_t, \mathbf{f}_t \sim Poi(\lambda_t), \quad \lambda_t = \exp(\boldsymbol{\theta}_t' \mathbf{F}_t). \quad (1)$$

To our best knowledge, this is the first study to treat the discrete time series within the BPS framework. Unlike the normal factor BPS model, the latent factors are in the exponential function. Since our COVID-19 hospitalisation data also include large counts, to avoid numerical instability, the predictive distribution of $\log y_t$ is used to construct h_{tj} .

Then, the normal density is used for h_{tj} to facilitate the posterior computation so that $f_{tj} \sim N(m_{tj}, s_{tj}^2)$. In Section 4, we describe how to obtain the means and variances of these normal densities for each agent.

For predicting the multiple time series count data, as the weekly number of COVID-19 inpatients of the prefectures of Japan, a multivariate BPS would improve the predictive performance over a univariate BPS (McAlinn et al., 2020). However, the specification and implementation of multivariate count time series models are generally cumbersome. Therefore, the choice of feasible multivariate models for agents and BPS that can be employed are quite limited. Based on the observation that our data exhibit a group of time series with similar dynamics, the proposed model introduced below partitions them into clusters based on the finite mixture of BPS. Through the clustering structure, we can leverage the shared information without resorting to a complex multivariate count model and also reduce the number of parameters to be estimated.

3.2 Mixture of Bayesian predictive syntheses

Now consider clustering and predicting n univariate time series count data denoted by $y_{it}, i = 1, \dots, n, t = 1, 2, \dots$, such as the number of inpatients in i th prefecture on t th day. To predict y_{it} , an analyst, again, elicits J models with the predictive density denoted by $h_{itj}(f_{itj}), j = 1, \dots, J$. The collection of J predictive densities form an information set denoted by $\mathcal{H}_{it} = (h_{it1}(\cdot), \dots, h_{itJ}(\cdot))$. The mixture of Bayesian predictive syntheses (MBPS) considers the following synthesised predictive distribution given by

$$p(y_{it} | \Phi_t, \mathcal{H}_{it}) = \int \left[\sum_{k=1}^K \pi_k \alpha(y_{it} | \mathbf{f}_{it}, \Phi_{tk}) \right] \left[\prod_{j=1}^J h_{itj}(f_{itj}) \right] d\mathbf{f}_{it}, \quad (2)$$

where $\sum_{k=1}^K \pi_k \alpha(y_{it} | \mathbf{f}_{it}, \Phi_{tk})$ is the mixture synthesis function whose k th component is denoted by $\alpha(\cdot | \mathbf{f}_{it}, \Phi_{tk})$, Φ_{tk} denotes the parameter of k th component including the vector of synthesis weights θ_{tk} , π_k is the component weight for k th synthesis function with $\sum_{k=1}^K \pi_k = 1$, and $\mathbf{f}_{it} = (f_{it1}, \dots, f_{itJ})'$ denotes the vector of the latent factors. With this

choice of the synthesis function, the synthesised predictive distribution (2) is rewritten as

$$\begin{aligned}
p(y_{it}|\Phi_t, \mathcal{H}_{i,1:t}) &= \sum_{k=1}^K \pi_k \int \alpha(y_{it}|\mathbf{f}_{it}, \Phi_{tk}) \left[\prod_{j=1}^J h_{itj}(f_{itj}) \right] d\mathbf{f}_{it} \\
&= \sum_{k=1}^K \pi_k p_k(y_{it}|\Phi_{tk}, \mathcal{H}_{i,1:t}).
\end{aligned} \tag{3}$$

Therefore, MBPS is the finite mixture of synthesised predictive distributions with the synthesis function in k th component given by

$$p_k(y_{it}|\Phi_{tk}, \mathcal{H}_{i,1:t}) = \int \alpha(y_{it}|\mathbf{f}_{it}, \Phi_{tk}) \left[\prod_{j=1}^J h_{itj}(f_{itj}) \right] d\mathbf{f}_{it}.$$

For two time series i and i' in the same cluster k , the mixture synthesis function places the same weight θ_{tjk} on j th model whose predictions are generally different between i and i' . The weights θ_{tk} are estimated from the set of time series belonging to the same cluster. In this way, MBPS leverages the shared information across time series based on the similarity in how each agent model contributes to the prediction.

The advantages of the proposed MBPS approach are as follows. Firstly, MBPS clusters the time series *after* synthesising the individual predictions from J agent models as in (2), thus clustering the synthesised predictive distributions. Alternatively, one could cluster the n time series within a subset of the agent models. However, this approach may be cumbersome since it requires determining the number of clusters for each agent clustering model.

Secondly, MBPS can reduce the number of parameters to be estimated. An alternative BPS approach that does not consider clustering would treat (y_{1t}, \dots, y_{nt}) as the multivariate time series as in McAlinn et al. (2020). In this case, the dimension of the weights is $n \times (J + 1)$ for each t . On the other hand, in MBPS, the dimension of the weights is $K \times (J + 1)$ for each t with K much smaller than n .

Related to the second point, each agent model fed into MBPS can be univariate. Then, these individual univariate predictions are combined through the mixture of synthesised predictive distributions. Since the construction and implementation of multivariate count models are generally cumbersome and univariate models are abundant, one can easily

choose and fit a set of univariate agent models and feed them into MBPS.

The model specification for each component is as follows. Since y_{it} is the count data, we use the Poisson probability mass function for α . By introducing the cluster assignment indicator denoted by $z_i \in \{1, \dots, K\}$, $i = 1, \dots, n$, we have the hierarchical form for MBPS given by

$$\begin{aligned} y_{it} | z_i = k, \boldsymbol{\theta}_{tk}, \mathbf{f}_{it} &\sim Poi(\exp(\boldsymbol{\theta}'_{tk} \mathbf{F}_{it})), \\ \Pr(z_i = k) &= \pi_k, \quad k = 1, \dots, K, \end{aligned} \tag{4}$$

where $Poi(\lambda)$ denotes the Poisson distribution with the mean λ and $\mathbf{F}_{it} = (1, \mathbf{f}'_{it})'$. Furthermore, the sparse Dirichlet prior distribution $Dir(a_0, \dots, a_0)$ with $a_0 < 1$ is assumed for $\boldsymbol{\pi} = (\pi_1, \dots, \pi_K)$ so that the similar components are merged and the weights for the redundant components are shrunk towards zero (Rousseau and Mengersen, 2011). As the default choice, we thus use $a_0 = 0.01$. Under this sparsity-inducing prior, we set $K = n$ in the real data analysis. As described in the previous subsection, by constructing the predictive distribution on the log scale, the normal densities are used for h_{itj} such that $f_{itj} \sim N(m_{itj}, s_{itj}^2)$. As in McAlinn and West (2019), $\boldsymbol{\theta}_{tk}$ is modelled as the normal random walk model:

$$\boldsymbol{\theta}_{tk} = \boldsymbol{\theta}_{t-1,k} + \mathbf{e}_{tk}, \quad \mathbf{e}_{tk} \sim N(\mathbf{0}, \boldsymbol{\Sigma}_{tk}), \quad k = 1, \dots, K. \tag{5}$$

The model is estimated by the Markov chain Monte Carlo (MCMC) algorithm. Specifically, we employ the approach of Hamura et al. (2021) to approximate the probability mass function of the Poisson distribution with that of the negative binomial distribution with a large dispersion parameter. Then the Pólya-gamma augmentation of Polson et al. (2013) is applied to obtain the conditionally linear Gaussian state space model to which the forward filtering and backward sampling algorithm (Frühwirth-Schnatter, 1994; West and Harrison, 1997) can be implemented. We introduce the common discount factors to facilitate the MCMC sampling through the dynamic linear model (DLM) updating scheme. The details are provided in Appendix.

3.3 Simultaneous clustering of synthesis weights and latent factors

The specification (4) can be modified to cluster both model weights and latent factors by introducing the following model:

$$\begin{aligned} y_{it}|z_i = k, \boldsymbol{\theta}_{tk}, \mathbf{f}_{it} &\sim Poi(\exp(\boldsymbol{\theta}'_{tk} \mathbf{G}_{tk})) \delta_{\mathbf{f}_{it}=\mathbf{g}_{tk}}, \\ \Pr(z_i = k) &= \pi_k, \quad k = 1, \dots, K, \end{aligned} \quad (6)$$

where $\delta_{\mathbf{f}_{it}=\mathbf{g}_{tk}}$ is a Dirac measure on $\mathbf{f}_{it} = \mathbf{g}_{tk}$, \mathbf{g}_{tk} is a vector of the unknown common latent factors among time series with $z_i = k$ and $\mathbf{G}_{tk} = (1, \mathbf{g}'_{tk})'$. In this case, while each time series has its own h_{itj} , the draws from h_{itj} are the same, \mathbf{g}_{tk} , for the series in the same cluster. Details of the MCMC algorithm are provided in Appendix.

3.4 Introducing heterogeneity in the intercept

The time series within a cluster of MBPS (2) have the same contribution from the agent models and the same level of inadequacy of their predictive performance, which is expressed by the intercept. However, it would be more helpful to introduce a little flexibility into the model by allowing the intercept to vary within a cluster. The extended model with the heterogeneity in the intercept is given by

$$\begin{aligned} y_{it}|z_i = k, \boldsymbol{\theta}_{tk}, \mathbf{f}_{it}, u_{it} &\sim Poi(\exp(\boldsymbol{\theta}'_{tk} \mathbf{F}_{it} + u_{it})), \\ u_{it}|z_i = k &\sim N(0, \tau_{tk}^2), \\ \tau_{tk}^2 &= \frac{\beta_\tau}{\gamma_t} \tau_{t-1,k}^2, \quad \gamma_t \sim Beta\left(\frac{\beta_\tau n_{t-1}}{2}, \frac{(1 - \beta_\tau) n_{t-1}}{2}\right). \end{aligned} \quad (7)$$

This model can be regarded as an intermediate model between the univariate BPS and MBPS (4). The additional random intercept u_{itk} captures the deviation from the cluster-specific constant θ_{tk0} . Its variance τ_{tk}^2 follows the beta-gamma random walk volatility model with the discount factor $\beta_\tau \in (0, 1]$ (see, for example, West and Harrison, 1997; Prado and West, 2010). We use the same Gaussian random walk model for $\boldsymbol{\theta}_{tk}$ as in (5). Details of the MCMC algorithm are provided in Appendix.

4 Analysis of COVID-19 inpatients and isolated cases

Here, the proposed MBPS methodology is demonstrated using the weekly numbers of COVID-19 inpatients in the prefectures of Japan and daily numbers of COVID-19 isolated cases in the metropolitan autonomous governments of Korea.

4.1 Agent models

We consider the following four agent models ($J = 4$): Poisson dynamic generalised linear model (DGLM), Poisson generalised additive model (GAM), Poisson integer autoregressive model (INAR) and Power-weighted Poisson model with the susceptible-infected-hospitalised-recovered compartment model (SIHR).

For DGLM, we assume $y_{it} \sim Poi(\exp(\mathbf{x}'_{it}\boldsymbol{\beta}_{it}))$ for $i = 1, \dots, n$ where $\mathbf{x}_{it} = (1, \tilde{I}_{it}, \tilde{I}_{it}^2)'$ and \tilde{I}_{it} is the log of the seven days lag of the 14 days moving average of the number of infected individuals. The time varying regression coefficient $\boldsymbol{\beta}_{it}$ is assumed to follow the random walk process, $\boldsymbol{\beta}_{it} = \boldsymbol{\beta}_{i,t-1} + \mathbf{u}_{it}$ where \mathbf{u}_{it} has the mean $\mathbf{0}$ and covariance \mathbf{W}_{it} . The model uses the standard DGLM updating scheme with the discount factor for \mathbf{W}_{it} (West et al., 1985; Berry and West, 2020).

For GAM, we assume $y_{it} \sim Poi(\lambda_{it})$, $\lambda_{it} = \exp(\beta_0 + s_{1i}(\tilde{I}_{it}) + s_{2i}(t))$ for $i = 1, \dots, n$ where β_0 is the constant term, and $s_{1i}(\tilde{I}_{it})$ and $s_{2i}(t)$ are the smooth functions of \tilde{I}_{it} and t , respectively, modelled through the smoothing spline. This model is implemented using the R package `gam`.

For INAR, we assume $y_{it}|y_{i,t-1} \sim Poi(\exp(\mathbf{x}'_{it}\boldsymbol{\beta}_i + \gamma_i y_{i,t-1}))$ where \mathbf{x}_{it} is the same as above. This model is implemented using the R package `tscount`.

Finally, the SIHR epidemic compartment model is considered. The SIHR model is chosen because it is reasonably simple and includes a compartment for hospitalisation or isolation. The power-weighted approach of McCarthy and Jensen (2016) discounts the past Poisson observations, which is regarded as a generalisation of the rolling window approach. Then, the Poisson means are modelled as the solution of the SIHR epidemic compartment model, obtained by the R package `deSolve`. Specifically, the power-weighted

likelihood function for the Poisson observations y_{i1}, \dots, y_{it} is given by

$$p(y_{i,1:t}|\lambda_{it}) = \prod_{s=1}^t \left[\frac{\lambda_{it}^{y_{is}} \exp(-\lambda_{it})}{y_{is}!} \right]^{a_s}, \quad t = 1, 2, \dots,$$

where λ_{it} is the mean parameter of the Poisson distribution and $a_s \in [0, 1]$ is the discount factor. In this approach, the Poisson observations y_{i1}, \dots, y_{it} have the common parameter λ_{it} , but the amount of their information used for the estimation of λ_{it} and prediction of $y_{i,t+1}$ is controlled by the discount factors a_1, \dots, a_t . In this paper, it is defined as $a_s = \delta_{SIHR}^{t-s}$ for $s = 1 \dots, t$ following Fisher et al. (2020). When δ_{SIHR} is different from one, the information of the observations further away from the time t is more discounted.

To construct h_{itj} , at the time $t-1$, we calculate the mean and variance of the predictive distribution individually for each agent, m_{itj} and s_{itj}^2 , given the information $y_{i,1:t-1}$ and \mathbf{x}_{it} , for the models with covariates. These quantities are calculated repeatedly as new information arrives. For DGLM, they can be obtained directly from the DGLM updating scheme because the linear predictor is also on the log scale. For the remaining three models, we use the parametric bootstrap to compute the predictive means and variances on the log scale. Then to predict y_{it} , one draws f_{itj} from $N(m_{itj}, s_{itj}^2)$ for $j = 1, \dots, J$, then given \mathbf{f}_{it} , $\boldsymbol{\theta}_{tzi}$ and z_i , we draw y_{it} from $Poi(\exp(\boldsymbol{\theta}'_{tzi} \mathbf{F}_{it}))$.

In addition to the four agent models, as suggested by one of the reviewers, we also consider the finite mixture of Poisson regression models, denoted by FMPR. This model is based on Zhu and Zhang (2004), which is also reviewed by Frühwirth-Schnatter (2011). While FMPR is not included in BPS as an agent, it would be interesting to compare the proposed BPS models with a model from a different class. The specification of FMPR is similar to that of our MBPS, but instead of latent factors from the agent models, it includes the observable covariates:

$$y_{it}|z_i = k \sim Poi(\exp(\mathbf{x}'_{it} \boldsymbol{\beta}_k)),$$

$$\Pr(z_i = k) = \pi_k, \quad k = 1, \dots, K$$

where $\mathbf{x}_{it} = (1, \tilde{I}_{it}, \tilde{I}_{it}^2, y_{i,t-1})'$. Assuming the prior distribution $\beta_k \sim N(\mathbf{0}, 100\mathbf{I})$, the model is estimated using the MCMC.

4.2 Performance measures

We compare the performance of the agent models, FMPR, and the proposed BPS model for univariate counts and three MBPS models. Hereafter, MBPS1 denotes the model with (4), MBPS2 denotes one with (6), and MBPS3 denotes the one with (7). The univariate BPS model is denoted by BPS when there is no confusion. The performance of the models is compared based on the following: the cumulative absolute prediction errors (CAPE) given by

$$\text{CAPE}_{it}^s = \sum_{t^*=T}^t |y_{i,t^*+s} - \hat{y}_{i,t^*+s}|,$$

the log predictive density ratio (LPDR) given by

$$\text{LPDR}_{it}^s = \log \frac{p_j(y_{i,t+s}|y_{i,1:t})}{p_{\text{MBPS1}}(y_{i,t+s}|y_{i,1:t})}, \quad t = T, \dots, T + T^* - s,$$

where $p_{\text{MBPS1}}(y_{t+s}|y_{1:t})$ and $p_j(y_{t+s}|y_{1:t})$ are the s -step-ahead predictive density of MBPS1 and other models, respectively, and the coverage of 95% prediction intervals given by

$$\text{Coverage}^s = \frac{1}{n(T^* - s)} \sum_{i=1}^n \sum_{t^*=T}^{T+T^*-s} \{L_{i,t^*+s} < y_{i,t^*+s} < U_{i,t^*+s}\}$$

The LPDR for j th model below zero implies the superiority of the proposed MBPS1, and that above implies the superiority of j th model over MBPS1. We also consider the total CAPE defined by $\sum_{i=1}^n \text{CAPE}_{it}^s$ and total LPDR defined by $\sum_{i=1}^n \text{LPDR}_{it}^s$.

4.3 Analysis of latent factors

Following McAlinn and West (2019), we compute the following measures to investigate the inter-dependency and redundancy in the agent predictions based on the latent factors inferred from the observed data. For each t , we compute the Monte Carlo (MC)-empirical R^2 for the latent factor for j th agent, f_{itj} , given the factors for all the other agents, $f_{itj'}$, $j' \neq j$ from the MCMC output. This R^2 measures the redundancy of j th agent in the context of all J agents for $j = 1, \dots, J$. We also compute the MC-empirical R^2 for each pair of j and j' , $j \neq j'$, to measure the pairwise dependence. It is called the paired MC-empirical R^2 .

4.4 Cluster determination

The MCMC algorithm described in Appendix provides the posterior sample of the cluster assignment, denoted by $\mathbf{z}^{(1)}, \dots, \mathbf{z}^{(L)}$ where $\mathbf{z}^{(\ell)} = (z_1^{(\ell)}, \dots, z_N^{(\ell)})$, $\ell = 1, \dots, L$. Following Nieto-Barajas and Contreras-Cristán (2014) and Lin et al. (2019), we select the most representative draw $\mathbf{z}^{(\ell^*)}$ from the MCMC output. To do so, define the $N \times N$ co-clustering matrix $\mathbf{Z}^{(\ell)}$ for $\ell = 1, \dots, L$ whose (i, j) entry is equal to one if $z_i^{(\ell)} = z_j^{(\ell)}$ and is equal to zero otherwise. We also define the mean co-clustering matrix $\hat{\mathbf{Z}} = L^{-1} \sum_{\ell=1}^L \mathbf{Z}^{(\ell)}$ which summarises the entire MCMC output. Then we select the ℓ^* -th draw $\mathbf{z}^{(\ell^*)}$ as the final clustering for which the Frobenius norm from the mean co-clustering matrix is minimised: $\ell^* = \arg \min_{\ell} \|\mathbf{Z}^{(\ell)} - \hat{\mathbf{Z}}\|_F$.

4.5 Analysis of weekly numbers of inpatients in Japan

The agent models are estimated using the first 50 weeks up to 14 April 2021. The BPS models are first run using the data from 21 April 2021 to 30 March 2022 ($T = 50$ weeks). Then, by expanding the window of the past data, the one-step-ahead predictions are obtained for both agent and BPS models from 6 April 2022 to 23 November 2022 ($T^* = 34$ weeks). All the discount factors for the agent and BPS models are set to 0.95 to account for the fast changes in the data.

4.5.1 Predictive performance

Figure 3 presents the prediction results under the agent models and MBPS, CAPE and LPDR for the selected prefectures, Hokkaido, Tokyo, Osaka and Fukuoka. The left panels of the figure show that the proposed MBPS1, MBPS3 and BPS perform reasonably well overall, tracking the fast-changing time series. The CAPE of these three models are comparable and are smaller than or at least comparable with those of the agent models. On the contrary, for the agent models, especially SIHR, there seems to be some lag in turning from a downward trend to an upward trend and vice versa, causing larger prediction errors. The predictions under the agent models tend to be larger than the observed data in the downward trend and smaller in the upward trend. When the number of inpatients peaked in August 2022, the predicted number of inpatients under FMPR was much larger than the

observed number. The performance of MBPS2, which clusters synthetic weights and latent factors, is inferior to that of the other MBPS and BPS models. The LPDR is negative for most of the prediction period, except for July of 2022, during which the number of inpatients turned into an upward trend towards the peak in August. There should not be a concern about this since the predictions under the agent models are generally higher than the observed trend before July, and they happen to become close to or cross the observed data in July, resulting in positive LPDR. For some periods, LPDR, especially for SIHR, was not obtained due to the underflow and thus, the curves are discontinuous during those periods.

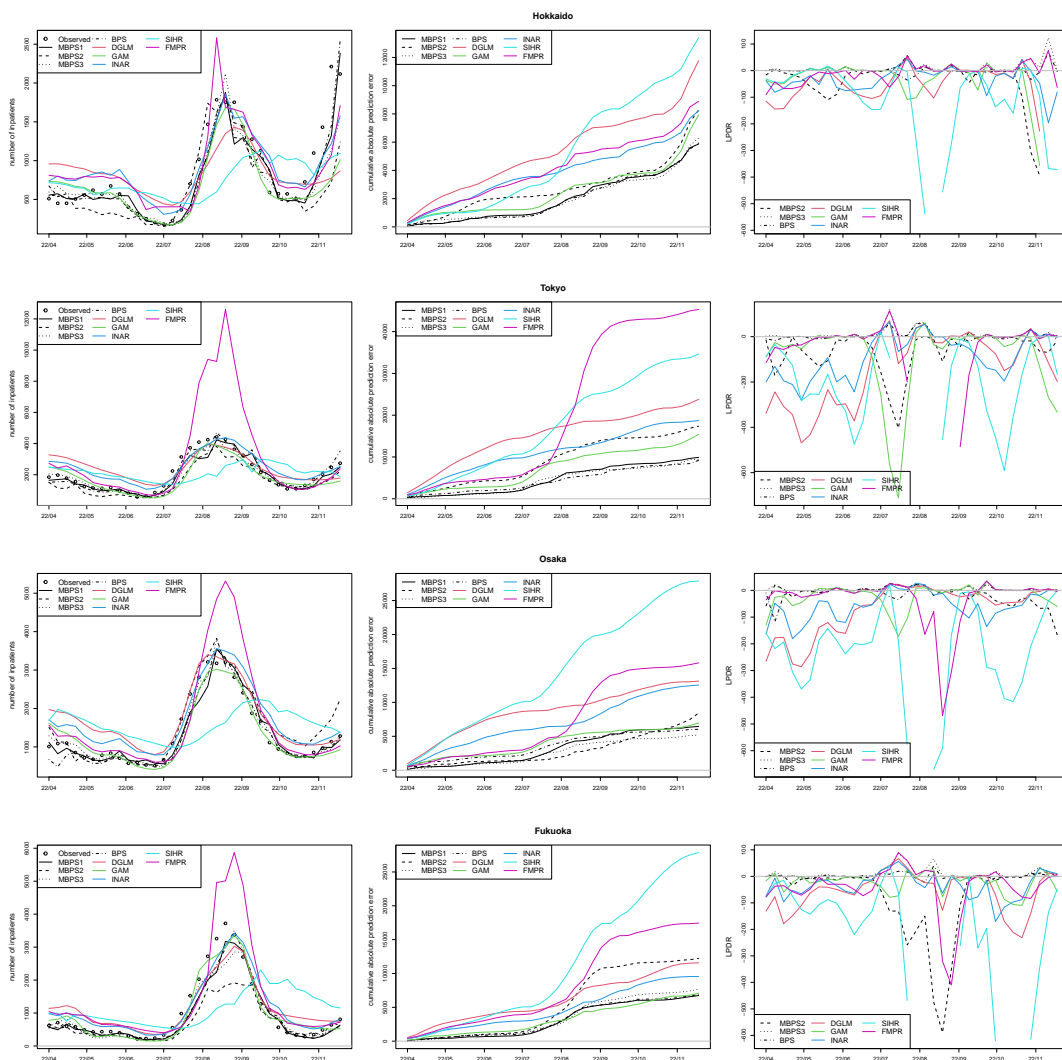


Figure 3: One-step-ahead prediction results (left), CAPE (middle) and LPDR (right) for the selected prefectures

Figure 4 presents the total CAPE and total LPDR, which are the CAPE and LPDR summed over the prefectures, as a summary of the overall performance of the models. It is seen that the total CAPE for MBPS1, MBPS3 and BPS are the lowest of the nine models, and they are comparable. The total CAPE for MBPS2 is comparable with GAM up to August 2022, but it becomes larger after that and is comparable with INAR at the end of the prediction period. The figure also shows that the total CAPE for SIHR is the largest at the end of the prediction period, followed by FMPR. The right panel of the figure shows that LPDR for the agent models and MBPS2 are negative for most of the prediction period, implying the superiority of MBPS1 over these models. On the other hand, LPDR for MBPS3 is positive throughout the prediction period.

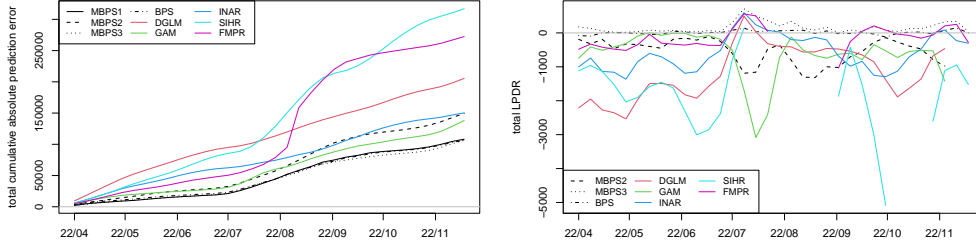


Figure 4: One-step-ahead CAPE (left) and LPDR (right) summed over prefectures

Table 3 presents the coverages of the 95% prediction intervals for one-step prediction. MBPS3 resulted in the coverage closest to the target value of 0.95. The other models resulted in undercoverage, and the coverages for the agent models and FMPR are particularly low, but some improvements by MBPS1 and BPS, which are comparative, over these models are also observed. This result highlights the severe difficulty in accurately predicting the number of COVID-19 inpatients. Appendix presents the results for the cases where the variances of the factors, s_{itj}^2 , in the BPS models, are deliberately inflated by five and times. However, the table shows little differences between the cases. In what follows, we mainly focus on MBPS3, which performs the best of the models considered here.

Table 1: Coverages of 95% prediction intervals for one-step-ahead prediction for Japanese data under the agents, FMPR and BPS models

MBPS1	MBPS2	MBPS3	BPS	DGLM	GAM	INAR	SIHR	FMPR
0.556	0.372	0.927	0.583	0.158	0.122	0.236	0.036	0.287

4.5.2 Analysis of latent factors

Following McAlinn and West (2019), we have a closer look at the posterior inference on the latent factors of MBPS3 given all data up to 23 November 2022. Figure 5 presents the posterior means of the latent factors, MC-empirical R^2 and paired MC-empirical R^2 for the same selected prefectures as in Figure 3. The left panels show that the posterior means of the latent factors, especially for DGLM, GAM and INAR, draw similar trajectories, albeit with some differences in amplitudes. This is reflected in the middle panels of the figure where the MC-empirical R^2 are very close to one. It is also seen that the predictability of SIHR, given others, drops during the peak period of August 2022, especially for Fukuoka. The paired R^2 are generally smaller than R^2 but are still above 0.6 in most of the prediction period for these prefectures.

The overall pattern in these measures can be more clearly seen by averaging over the prefectures, as presented by Figure 6. The average MC-empirical R^2 are generally high, between 0.8 and 1, throughout the prediction period, as shown in the left panel. The average R^2 for SIHR is slightly low compared to the others during the peak period of August 2022. It is also seen that the average R^2 for all agents dropped in September 2022, indicating some degree of disagreement among the agents on predicting when the peak has passed. The right panel of the figure shows that the average R^2 for the pairs DGLM-SIHR, GAM-SIHR and INAR-SIHR are low compared to the rest of the pairs in the peak period. It is also seen that the average paired R^2 dropped before and after the peak, July 2022 and September 2022.

4.5.3 Single agent method with different features

We investigate the cases where the agent models in a BPS model are confined within a single model class but with different features rather than using four different methods. This is also done in Takanashi and McAlinn (2023). More specifically, under MBPS3, we

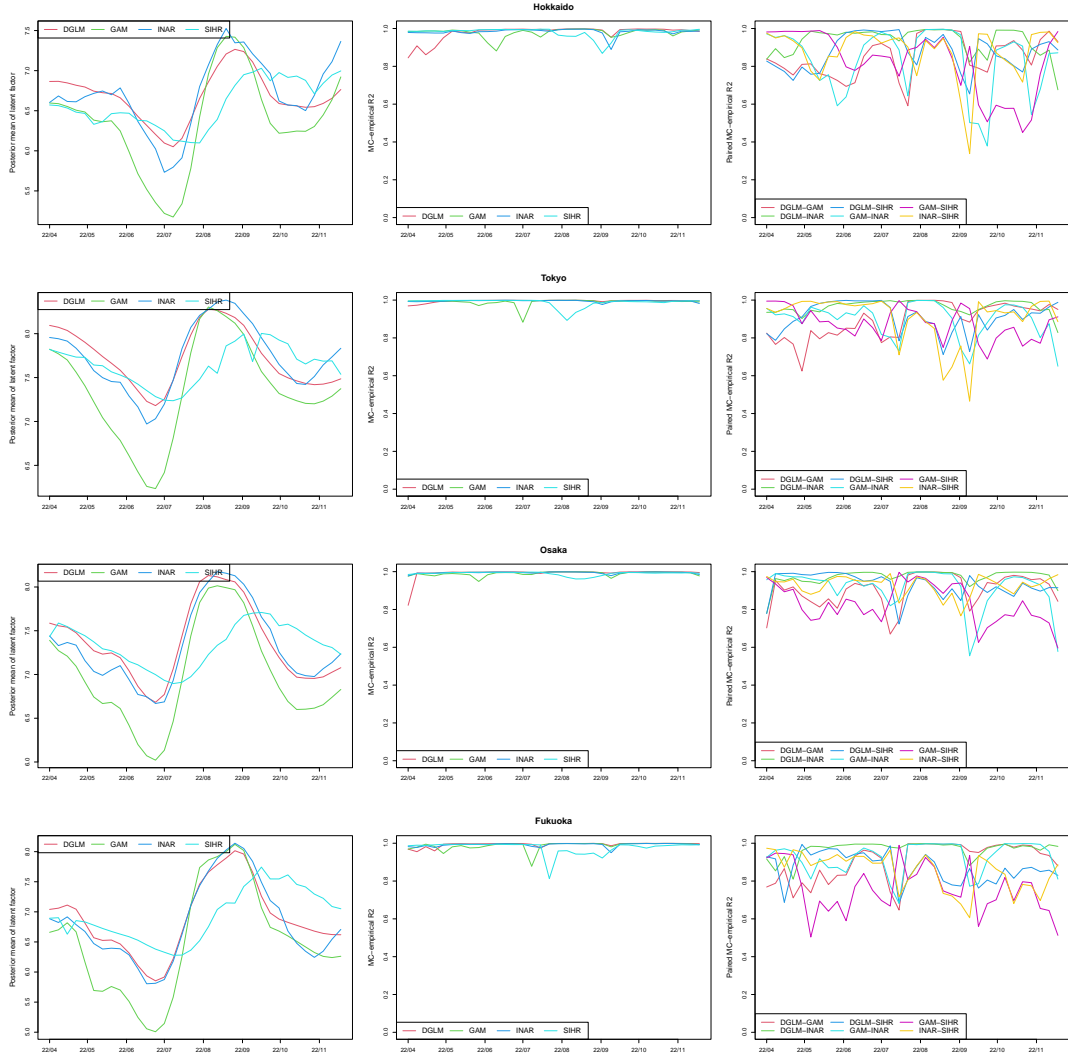


Figure 5: Posterior means of the latent factors f_{itj} (left), MC-empirical R^2 (middle) and paired MC-empirical R^2 (right) under MBPS3 for the selected prefectures given all Japanese data

consider the following three cases. In the first case, MBPS3 uses three DGLM with different set of covariates as agents, denoted by DGLM1 with $\mathbf{x}_{it} = 1$, DGLM2 with $\mathbf{x}_{it} = (1, \tilde{I}_{it})'$ and DGLM3 with $\mathbf{x}_{it} = (1, \tilde{I}_{it}, \tilde{I}_{it}^2)'$. In the second case, MBPS3 uses three GAM with the different mean functions as agents, denoted by GAM1 with $\lambda_{it} = \exp(\beta_0 + s_{1i}(\tilde{I}_{it}))$, GAM2 with $\lambda_{it} = \exp(\beta_0 + s_{2i}(t))$ and GAM3 with $\lambda_{it} = \exp(\beta_0 + s_{1i}(\tilde{I}_{it}) + s_{2i}(t))$. Finally, we consider MBPS3 with three INAR with different covariates as agents. The setting for the covariates is the same as that for DGLM. In this case, the corresponding agents are denoted by INAR1, INAR2 and INAR3. MBPS3-DGLM, MBPS3-GAM and MBPS3-INAR denote these specifications for MBPS3.

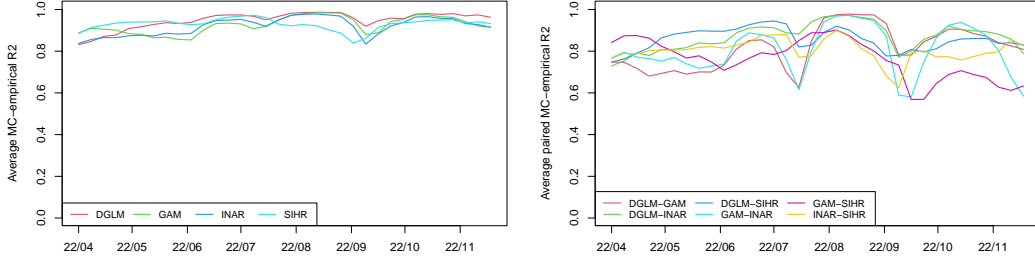


Figure 6: MC-empirical R^2 (left) and paired MC-empirical R^2 (right) averaged over prefectures given all Japanese data

Figure 7 presents the total CAPE in the three cases. The figure also plots the total CAPE for MBPS3 with four different agent methods shown in grey in Figure 4. In all cases, the original MBPS3 resulted in the lowest total CAPE. In each case, the agent model with the smallest set of covariate information resulted in the largest CAPE. For DGLM and INAR, the results for DGLM2 and DLMG3, as well as those for INAR2 and INAR3, are comparable, implying that the smaller sets of covariates may be sufficient. For GAM, MBPS3-GAM is comparable with GAM3. The result shown in Figure 7 suggests that including and combining various possible predictions in a BPS model is more effective than limiting the agent method to a single class.

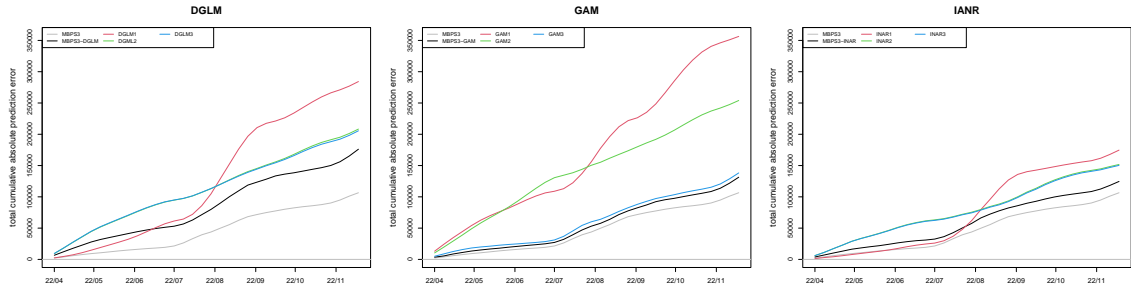


Figure 7: Total CAPE for MBPS3 with four different agent methods and MBPS3 with the agents in a single model class with different features for Japanese data

4.5.4 Clustering results

Figure 8 presents the clustered prefectures and posterior means of the synthesis weights based on the clustering results under MBPS3 using all data up to 23 November 2022.

Although a geographical interpretation of the clustering result may not be straightforward as MBPS clusters the prefectures based on the contribution of the agent models, we notice that the prefectures with similar magnitudes in the time series happened to form a cluster. Cluster I includes Tokyo and Osaka. Cluster H includes three prefectures, Chiba, Saitama and Kanagawa, which are neighbours of Tokyo. Cluster A includes Hokkaido, Aichi and Fukuoka, and Cluster B includes Gifu, Kyoto, Hiroshima and Okinawa. The prefectures in these clusters incurred large numbers of inpatients, as shown in the bottom panels of Figure 1.

In the bottom panels of Figure 8, the posterior means of the synthesis weights exhibit smooth trajectories with different levels for different clusters. For the constant term, Cluster H resulted in the largest values, followed by Cluster I, indicating the difficulty in predicting for the prefectures with large numbers of inpatients. For DGLM, the weights for most clusters are negative, and Clusters I and J resulted in the largest magnitudes. GAM has a large predictive contribution in Clusters A, F, H and K. On the contrary, the posterior means are close to zero for Cluster D, which is the singleton cluster of Okayama. The weights for INAR are positive and generally large for all clusters. Cluster I resulted in the largest posterior means, followed by Cluster D, B and H. For SIHR, Cluster I resulted in the posterior means of the largest magnitudes. Again, the number of inpatients is challenging to predict, so allowing negative weights in an agent model with poor predictive performance might improve the overall performance of BPS.

Figure 9 presents the scatter plot of the log averages of the time series, $\log(T^{-1} \sum_{t=1}^T y_{it})$, and average absolute values of the rates of changes from previous weeks in the time series, $T^{-1} \sum_{t=2}^T |y_{it} - y_{i,t-1}|/y_{i,t-1}$, to gain more insight on the characteristics of the clustered time series in terms of the level and smoothness of the series. It is first seen that the locations of the series belonging to the same cluster are similar. As described above regarding Figure 8, the levels of the time series appear to be an important factor in the clustering of MBPS. It is also seen that the clusters with large numbers of inpatients, such as Clusters A, H and I, located in the bottom right corner of the figure, are also associated with relatively low rates of changes compared to the rest of the clusters. Since GAM includes the smooth function of the number of infected individuals and time index, we expected that the clusters with large magnitudes of synthesis weights for GAM, such as Clusters A,

would be associated with low rates of changes in the time series. However, it is difficult to recognise such a pattern in the figure.

Finally, Figure 10 shows the numbers of the determined clusters under MBPS3 over the data period. The figure shows that the numbers of alive clusters do not vary significantly. The average number of clusters is 10.7.

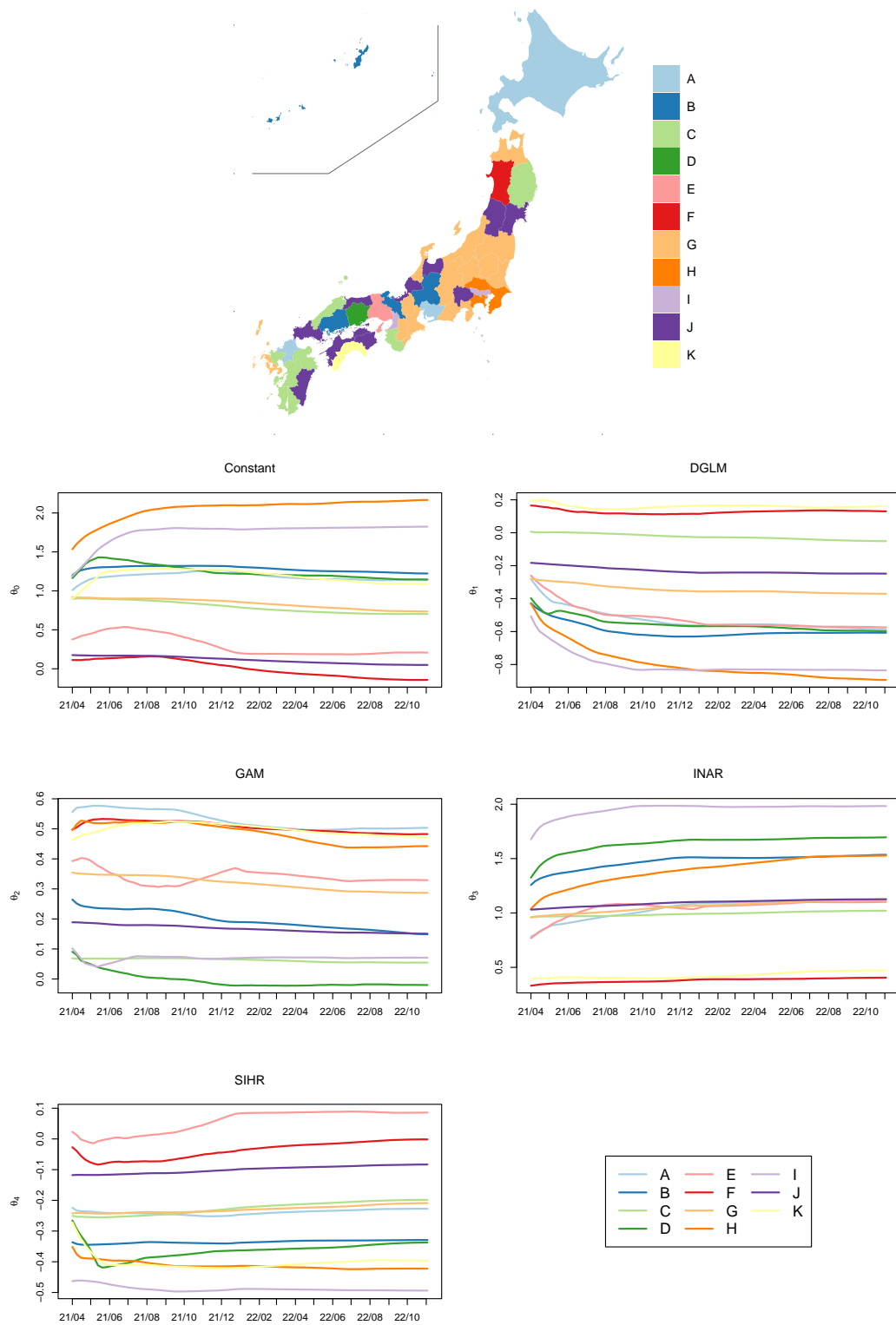


Figure 8: Clustered prefectures (top map), posterior means of the synthesis weights under MBPS3 (bottom panels) given all Japanese data

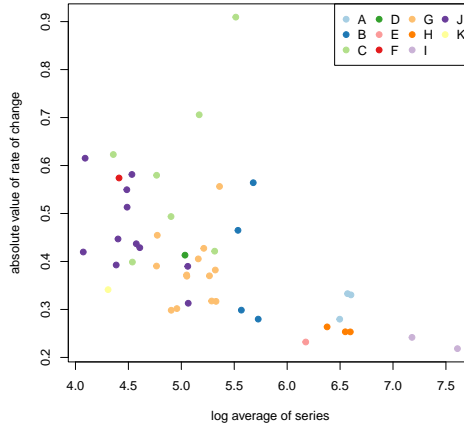


Figure 9: Profile of the clustered time series for the Japanese data given all data

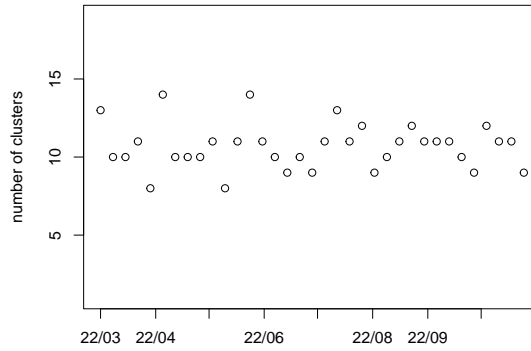


Figure 10: Numbers of clusters under MBPS3 for the Japanese data

4.6 Analysis of daily isolated cases in Korea

As in the previous analysis, the same four agent models are considered and are first estimated using the first three months of the data up to 31 October 2020. MBPS is fit using the data from 1 November 2020 to 31 July 2021 ($T = 273$ days) and then by expanding the window of the past data, the one-, three- and seven-step-ahead ($s = 1, 3, 7$) predictions from 1 August 2021 to 30 November 2021, are obtained ($T^* = 122$ days).

The multistep-ahead forecasts of MBPS are based on the customised BPS approach proposed by McAlinn and West (2019). Specifically, for predicting y_t at time $t-s$, BPS includes the s -step-ahead predictions of the agent models $h_{i,t-s,j}(f_{itj})$ rather than $h_{itj}(f_{itj})$. While the horizon-specific BPS model has to be estimated for each prediction horizon,

it directly relates the outputs from the agent models to the horizon s of interest. The discount factors for the agent and BPS models are set to 0.99.

4.6.1 Predictive performance

Figure 11 presents the prediction results, CAPE and LPDR for $s = 1, 3$ and 7 under the agent and proposed models for Seoul. The LPDR is shown only for MBPS3, BPS and INAR for visibility. In the left panels of Figure 11, MBPS2, SIHR, and FMPR clearly fail to predict the number of isolated cases. These panels especially show that the prediction under MBPS2 is highly unstable due to its restrictive model structure. The middle panels of Figure 11 show that CAPE for MBPS1, MBPS3, BPS and INAR are comparable throughout the prediction period in the cases of $s = 1$ and 3. More specifically, CAPE for BPS and INAR are slightly smaller than those for MBPS1 and MBPS3. In the case of $s = 7$, BPS resulted in the smallest CAPE, followed by MBPS1, INAR and MBPS3. In the right panels, LPDR for INAR exhibits occasional downward spikes, particularly around the mild peak in October 2021 and towards the end of the prediction period, especially for $s = 7$. These indicate the superiority of the BPS models over INAR. Between MBPS1 and MBPS3 or BPS, the figure also shows the notable upward spikes in LPDR in October 2021, indicating MBPS3 and BPS performed better than MBPS1 in capturing this mild peak in the number of isolated individuals.

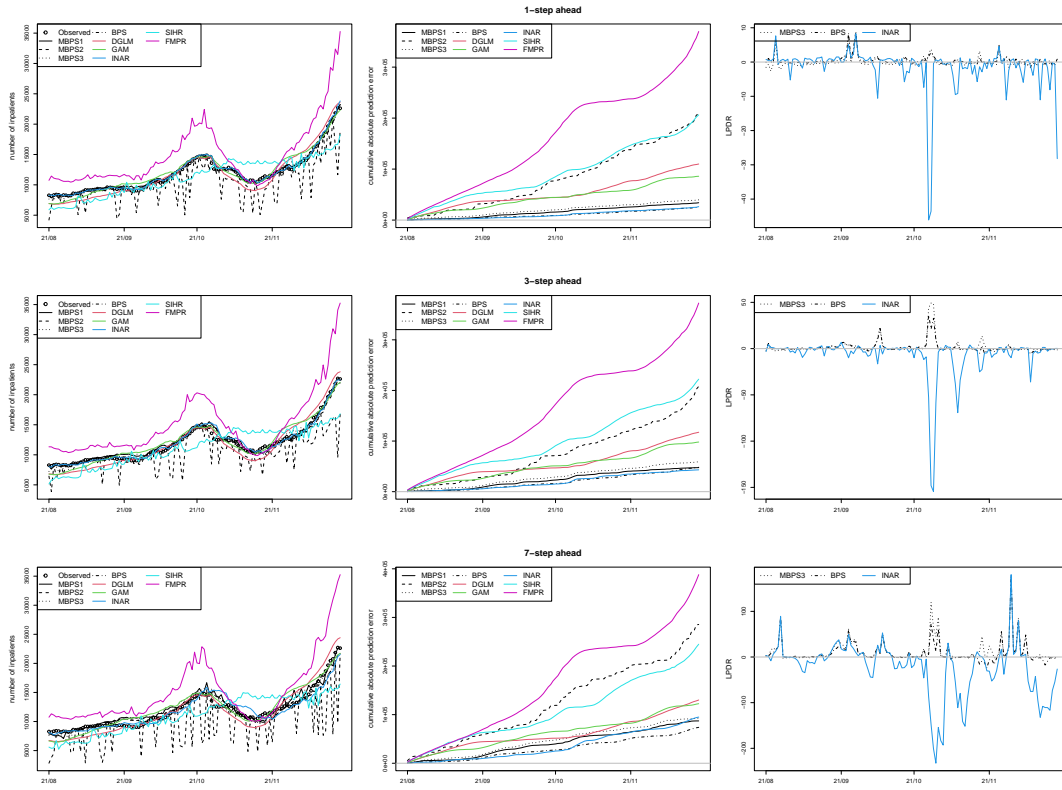


Figure 11: One-, three- and seven-step-ahead prediction results (left), CAPE (middle) and LPDR (right) for Seoul

Figure 12 shows the CAPE and LPDR summed over MAGs. For visibility, again, the total LPDR is shown only for MBPS3, BPS and INAR. In the cases of $s = 1$ and 3, the total CAPE for MBPS1, MBPS3, BPS and INAR appear comparable. In the case of $s = 7$, BPS resulted in a smaller total CAPE followed by MBPS1 and MBPS3. Similar to Figure 11, MBPS2, SIHR and FMPR are the models with the largest total CAPE. Turning to total LPDR, in the case of $s = 1$, MBPS3 and BPS are comparable throughout the prediction period. On the other hand, the total LPDR for INAR drops in the second half of the prediction period after October 2021. In the cases of $s = 3$ and 7, MBPS3 tends to result in the highest total LPDR, followed by BPS. The total LPDR for INAR is negative for most of the prediction period, implying the superiority of the BPS models over INAR.

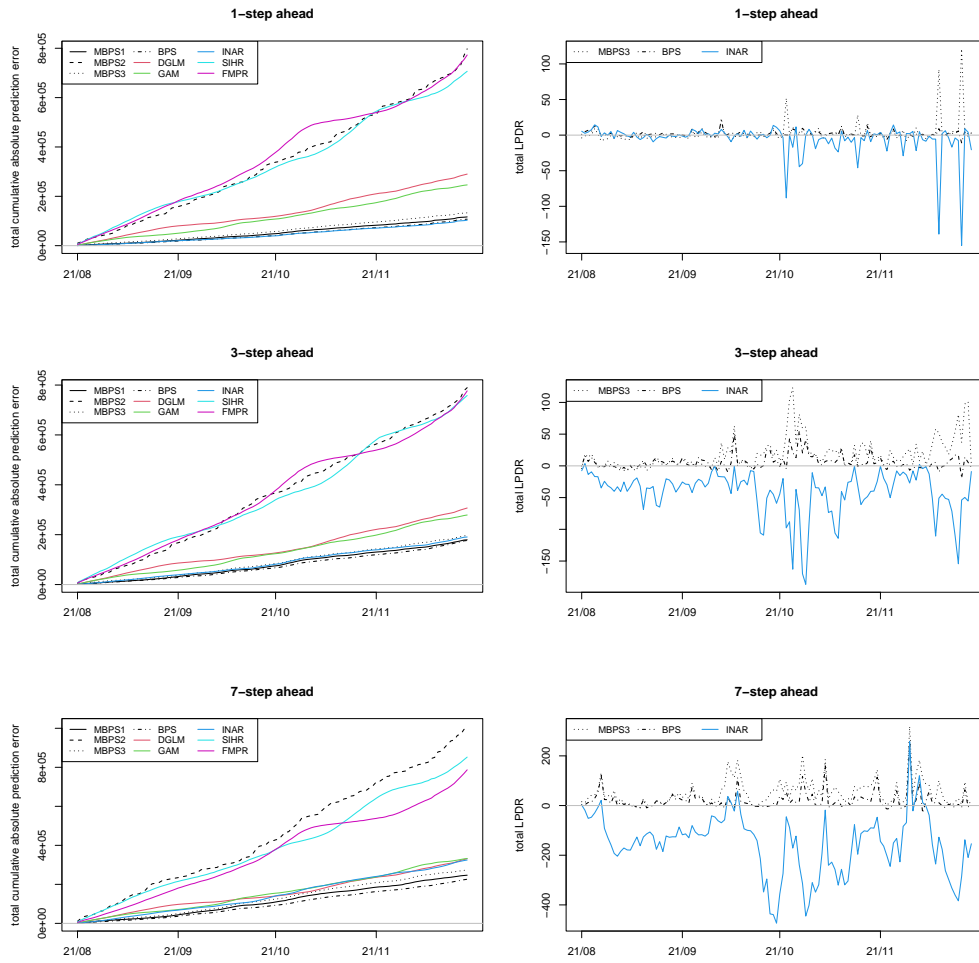


Figure 12: One-, three- and seven-step-ahead total CAPE (left) and total LPDR (right) for the Korean data

Table 2 shows the coverages of 95% prediction intervals. Most models resulted in undercoverage, especially in the case of $s = 7$, again indicating the difficulty of accurately predicting isolated COVID-19 cases. Nonetheless, MBPS3 resulted in the coverages closest to the target value of 0.95 in all the cases, followed by BPS and MBPS1. We also implemented the BPS models by inflating the variances of the latent factors by five, but we obtained similar results as in the case of the Japanese data. See Appendix.

4.6.2 Analysis of latent factors

Figure 13 presents the MC-empirical R^2 and paired MC-empirical R^2 for one-, three- and seven-step ahead prediction averaged over MAGs given all Korean data up to up to 30

November 2021. The left panes show that the R^2 for DGLM and GAM are almost identical and are close to one, indicating high conditional dependence in all cases. The R^2 for INAR and SIHR are lower than those for DGLM and GAM. The levels of R^2 do not seem to vary over the different prediction horizons. It is also seen in the three- and seven-step ahead prediction. R^2 for all models dropped at the beginning of October 2021. In the right panels, we observe similar patterns in the paired R^2 over the different prediction horizons. The paired R^2 for the DGLM-GAM pair are also the highest of all pairs, as shown in the right panels. Those for the DGLM-INAR and GAM-INAR pairs exhibit similar behaviour, as GAM and DGLM produced similar prediction results shown in Figure 12.

Table 2: Coverages of 95% prediction intervals for one-, three-, seven-step-ahead prediction for the Korean data

	MBPS1	MBPS2	MBPS3	BPS	DGLM	GAM	INAR	SIHR	FMPR
$s = 1$	0.918	0.286	0.964	0.932	0.605	0.169	0.848	0.028	0.351
$s = 3$	0.724	0.250	0.944	0.767	0.590	0.164	0.654	0.022	0.354
$s = 7$	0.637	0.248	0.953	0.697	0.575	0.169	0.456	0.028	0.360

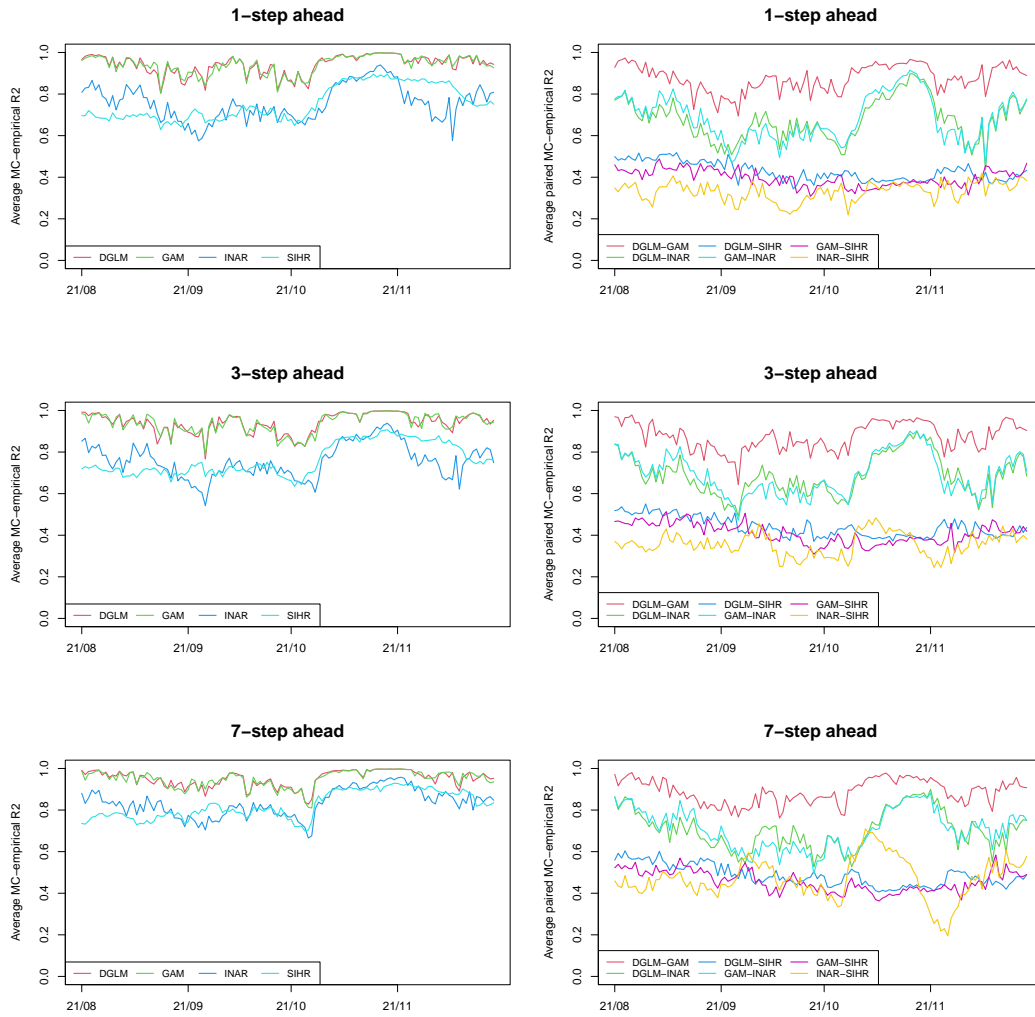


Figure 13: MC-empirical R^2 (left) and paired MC-empirical R^2 (right) under MBPS3 averaged over MAGs given all Korean data

4.6.3 Clustering results

Figure 14 presents the clustered MAGs and posterior means of the synthesis weights for $s = 7$ based on the clustering results under MBPS3 using all Korean data up to 30 November 2021. Due to space limitation, the results for $s = 1$ and 3 are presented in Appendix. It is shown that there are three clusters. Cluster A includes Seoul and its neighbours, Incheon and Gyeonggi-do. The levels of the time series for these MAGs are the highest in our data, as shown in Figure 2. Cluster b includes Jeollabuk-do, Chungcheongbuk-do, Gangwon-do, Busan, Gyeongsangbuk-do and Jeollanam-do, whose levels are next to those of MAGs in

Cluster a. Therefore, the clusters are associated with the levels of the time series, as in the result of the Japanese data analysis in Section 4.5.4. We also observe a similar pattern in the case of $s = 3$, while the pattern is unclear in the case of $s = 1$.

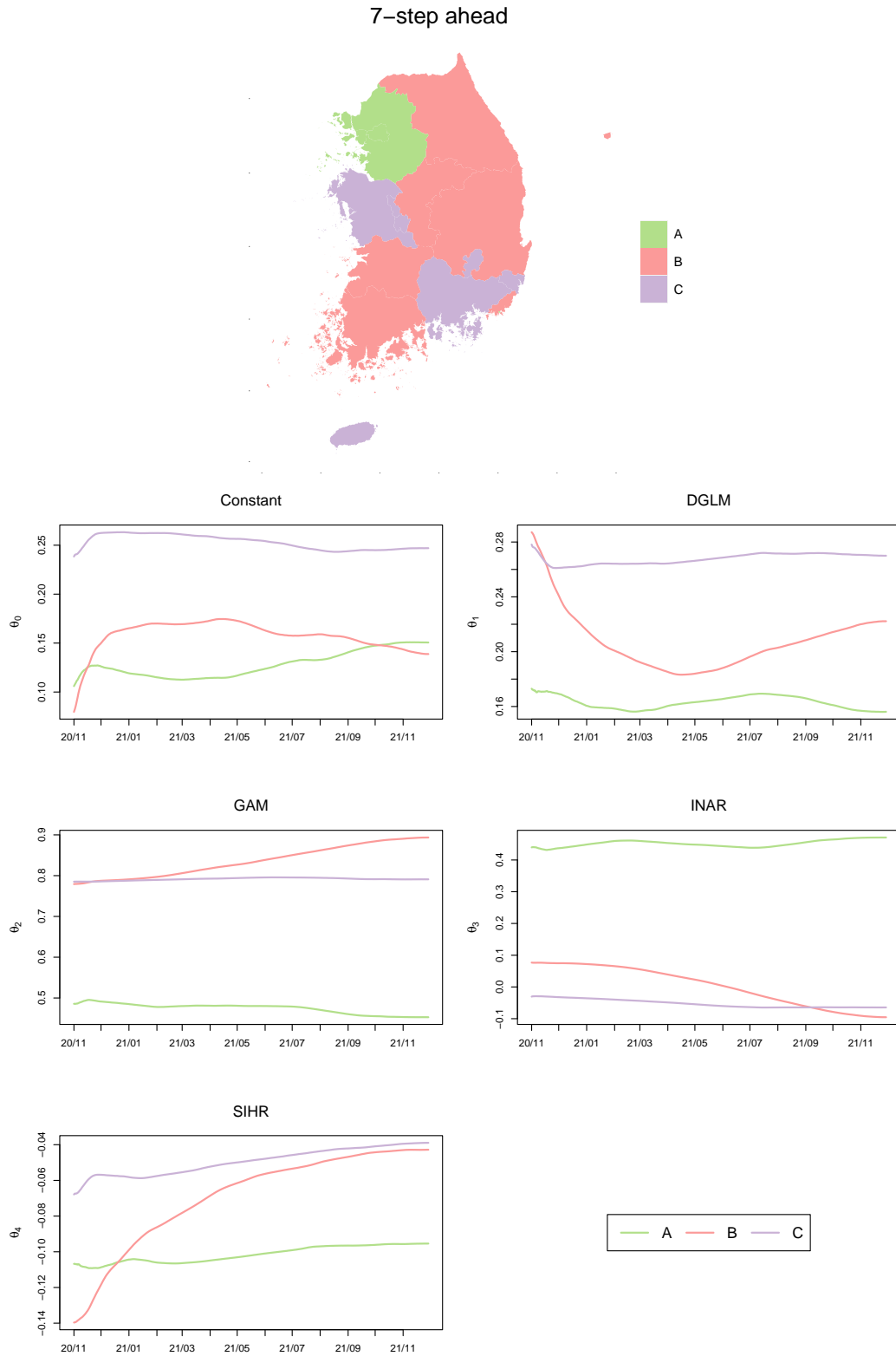


Figure 14: Clustered MAGs (top maps) and posterior means of the synthesis weights under MBPS3 for seven-step ahead prediction (bottom panels) given all Korean data

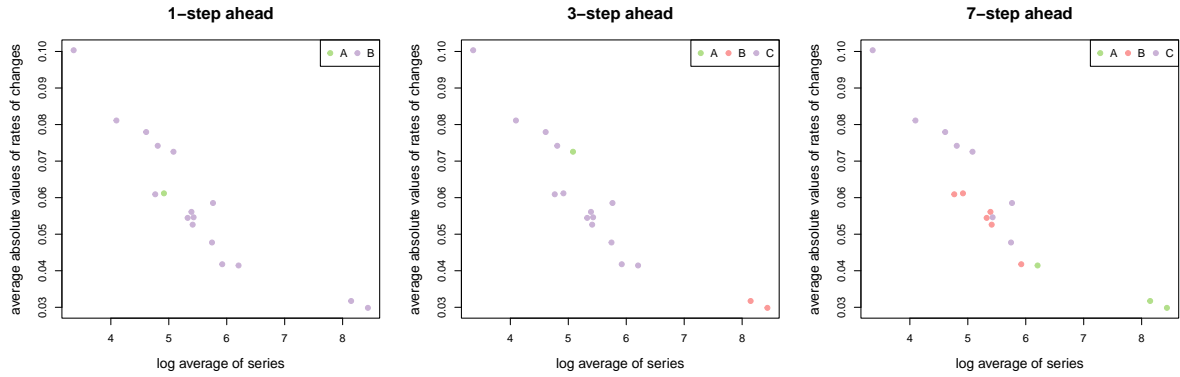


Figure 15: Profile of the clustered time series given all Korean data

In the bottom panels of Figure 14, Cluster C has the largest synthesis weight for DGLM. The trajectory of the weight for DGLM for Cluster B is in a U-shape, with the weight decreasing towards May 2021 and increasing towards the end of the data period. For GAM, the synthesis weights are relatively high for all clusters, especially for Clusters B and C. The weight for Cluster B is increasing towards the end of the data period. On the contrary, for INAR, Cluster A constantly has the highest synthesis weight, and the weight for Cluster C is constantly close to zero. The synthesis weights for SIHR are relatively close to zero for all clusters.

Figure 15 presents the scatter plot of the log averages of the time series and average absolute values of the rates of changes from previous weeks in the time series. The locations of the series that belong to the same cluster are similar in the cases of $s = 3$ and 7 . As in the observations above, the clusters are related to the levels of the time series. The figure also shows that time series with higher levels are associated with higher degrees of smoothness, such as the series in Cluster A in the case of $s = 7$ and those in Cluster B in the case of $s = 3$.

Finally, Figure 16 shows the numbers of clusters under MBPS3 over the data period. As in the case of Japanese data, the numbers of clusters are stable over the data period. The average numbers of clusters are 2.7, 3.1 and 3.7 for $s = 1$, 3 and 7, respectively. Therefore, the number of clusters tends to increase with the prediction horizon.

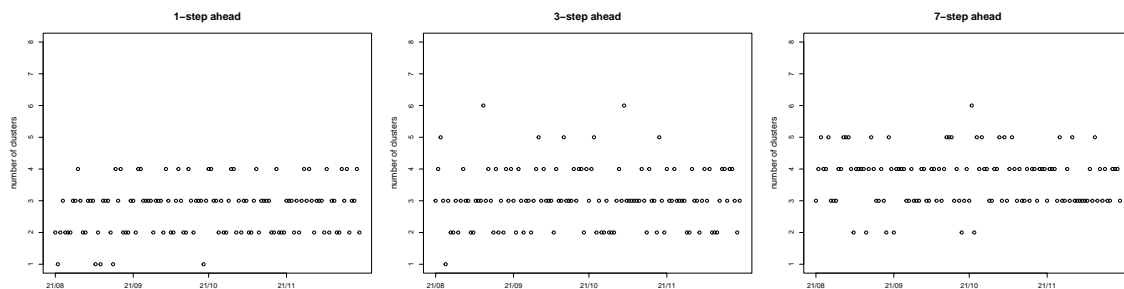


Figure 16: Numbers of alive clusters under MBPS3 for the Korean data

5 Conclusion

We have proposed the novel BPS methodology, the mixture of Bayesian predictive syntheses and variants, for multiple time series count data. The advantages of MBPS include the smaller number of BPS parameters and latent variables than the multivariate BPS and the use of univariate agent models. MBPS is particularly useful in multiple discrete time series analyses since the specification and implementation of a multivariate count model are generally cumbersome. The analysis of the Japanese and Korean data on the number of COVID-19 inpatients and isolated cases, respectively, showed that MBPS has improved predictive performance. The results also suggest that BPS is an effective statistical methodology that provides vital information for policy-making against infectious diseases.

In the real data analysis, we experienced the sudden failure of an agent model while the synthesis weights remained high due to sudden surges and drops in the COVID-19 data. This may amplify the deterioration of the predictive performance of MBPS. Since this problem is not specific to MBPS only, including a fail-safe mechanism within BPS would improve the performance of the BPS methodology and expand its applicability. We would like to explore the possible extension of BPS in this direction in future studies.

Acknowledgement

This work was supported by JSPS KAKENHI (#22K01421, #21K01421, #21H00699, #20H00080) and Japan-Korea Basic Scientific Cooperation Program between JSPS and NRF (#120218806). The research of Taeryon Choi was supported under the framework

of international cooperation program managed by the National Research Foundation of Korea (#2021K2A9A2A08000094, #FY2021).

A Posterior computation

A.1 Gibbs sampler for MBPS1

The posterior inference is carried out by using the Markov chain Monte Carlo (MCMC) method. In order to facilitate the MCMC sampling, we follow the approach of Hamura et al. (2021) and D'Angelo and Canale (2022) to approximate the Poisson pmf by the negative binomial pmf $\tilde{\alpha}(y_{it}|\mathbf{f}_{it}, \boldsymbol{\theta}_{tk}, r)$ with a large dispersion parameter r and then apply Pólya-gamma (PG) mixture of Polson et al. (2013). For a sufficiently large r , we have

$$\begin{aligned} \alpha(y_{it}|\mathbf{f}_{it}, \boldsymbol{\theta}_{tk}) &\approx \tilde{\alpha}(y_{it}|\mathbf{f}_{it}, \boldsymbol{\theta}_{tk}, r) \\ &= \frac{\Gamma(y_{it} + r)}{\Gamma(r)y_{it}!} \frac{(e^{\psi_{itk}})^{y_{it}}}{(1 + e^{\psi_{itk}})^{y_{it}+r}} \\ &= \frac{\Gamma(y_{it} + r)}{\Gamma(r)y_{it}!} 2^{-b_{it}} \exp\{\kappa_{it}\psi_{itk}\} \int_0^\infty \exp\left\{-\frac{\omega_{itk}\psi_{itk}^2}{2}\right\} p(\omega_{itk}|b_{it}, 0) d\omega_{itk}, \end{aligned}$$

where $b_{it} = y_{it} + r$, $\kappa_{it} = (y_{it} - r)/2$, $\psi_{itk} = \boldsymbol{\theta}'_{tk}\mathbf{F}_{it} - \log r$ and ω_{itk} follows the PG distribution $PG(b_{it}, 0)$ with the density $p(\omega_{itk}|b_{it}, 0)$. Throughout this paper, $r = 1000$ is used. See also D'Angelo and Canale (2022) for a data-driven approach to determine the value of r .

Then the joint distribution of the parameters and latent variables for $t = 1, \dots, T$ is proportional to

$$\begin{aligned} p(\boldsymbol{\pi}) \prod_{t=1}^T p(\boldsymbol{\theta}_{tk}|\boldsymbol{\theta}_{t-1,k}, \boldsymbol{\Sigma}_{tk}) \\ \times \left(\prod_{i=1}^n \left[\pi_k \exp\{\kappa_{it}\psi_{itk}\} \exp\left\{-\frac{\omega_{itk}\psi_{itk}^2}{2}\right\} p(\omega_{itk}|b_{it}, 0) \right]^{I(z_i=k)} \prod_{j=1}^J h_{itj}(f_{itj}) \right), \end{aligned} \quad (8)$$

where $p(\boldsymbol{\pi})$ is the prior density for $\boldsymbol{\pi}$ and $I(\cdot)$ is the indicator function. Then, our Gibbs sampler alternately samples $\{z_i\}$, $\{\boldsymbol{\theta}_{tk}\}$, $\{\mathbf{f}_{it}\}$, $\{\omega_{itk}\}$, $\{s_{ik}\}$ and $\boldsymbol{\pi}$.

Sampling z_i : For $i = 1, \dots, n$, z_i is sampled from the categorical distribution with probabilities proportional to $\Pr(z_i = k|\text{Rest}) \propto \pi_k \prod_{t=1}^T \alpha(y_{it}|\mathbf{f}_{it}, \boldsymbol{\theta}_{tk}, r)$ for $k = 1, \dots, K$.

Sampling $\boldsymbol{\pi}$: The full conditional distribution of $\boldsymbol{\pi}$ is the Dirichlet distribution $Dir(a_0 + \sum_i s_{i1}, \dots, a_0 + \sum_i s_{iK})$.

Sampling ω_{itk} : For $i = 1, \dots, n, t = 1, \dots, T$, ω_{itz_i} is sampled from $PG(r + y_{it}, \boldsymbol{\theta}'_{tz_i} \mathbf{F}_{it} - \log r)$.

Sampling \mathbf{f}_{it} : Let us define $\boldsymbol{\theta}_{-0,tk} = (\theta_{tk1}, \dots, \theta_{tkJ})$. From (8), the full conditional distribution of \mathbf{f}_{it} is proportional to

$$\begin{aligned} p(\mathbf{f}_{it} | \text{Rest}) &\propto \exp\{\kappa_{it}\psi_{itz_i}\} \exp\left\{-\frac{\omega_{itz_i}\psi_{itz_i}^2}{2}\right\} \prod_{j=1}^J h_{itj}(f_{itj}) \\ &\propto \exp\left\{-\frac{1}{2}(\mathbf{f}'_{it}\omega_{itz_i}\boldsymbol{\theta}_{-0,tz_i}\boldsymbol{\theta}'_{-0,tz_i}\mathbf{f}_{it} - 2(\omega_{itz_i}(\log r - \theta_{tz_i0}) + \kappa_{it})\mathbf{f}'_{it}\boldsymbol{\theta}_{-0,tz_i})\right\} \\ &\quad \times \prod_{j=1}^J h_{itj}(f_{itj}) \end{aligned}$$

Then, assuming that $h_{itj}(\cdot)$ is given by the density of $N(m_{itj}, s_{itj}^2)$ for $j = 1, \dots, J$, \mathbf{f}_{it} is sampled from $N(\hat{\mathbf{m}}_{it}, \hat{\mathbf{S}}_{it})$ where

$$\hat{\mathbf{m}}_{it} = \hat{\mathbf{S}}_{it} \left[\left(\omega_{itz_i}(\log r - \theta_{tz_i0}) + \frac{y_{it} - r}{2} \right) \boldsymbol{\theta}_{-0,tz_i} + \mathbf{S}_{it}^{-1} \mathbf{m}_{it} \right], \quad \hat{\mathbf{S}}_{it} = [\omega_{itz_i} \boldsymbol{\theta}_{-0,tz_i} \boldsymbol{\theta}'_{-0,tz_i} + \mathbf{S}_{it}^{-1}]^{-1},$$

for $i = 1, \dots, n, t = 1, \dots, T$, where $\mathbf{m}_{it} = (m_{it1}, \dots, m_{itJ})'$ and $\mathbf{S}_{it} = \text{diag}(s_{it1}^2, \dots, s_{itJ}^2)$.

Sampling $\boldsymbol{\theta}_{tk}$: Let us define $n_k = \sum_{i=1}^n I(z_i = k)$, which is the number of time series belonging to k th cluster. From (8), we have

$$p(\boldsymbol{\theta}_{1:T,k} | \text{Rest}) \propto \prod_{t=1}^T \exp\left\{-\frac{1}{2}(\mathbf{d}_{tk} - \mathbf{F}_{tk}\boldsymbol{\theta}_{tk})' \boldsymbol{\Omega}_{tk} (\mathbf{d}_{tk} - \mathbf{F}_{tk}\boldsymbol{\theta}_{tk})\right\} p(\boldsymbol{\theta}_{tk} | \boldsymbol{\theta}_{t-1,k}, \boldsymbol{\Sigma}_{tk}),$$

where for i such that $z_i = k$, the $n_k \times 1$ vector \mathbf{d}_{tk} is the collection of $(y_{it} - r)/2\omega_{itk} + \log r$, the rows of the $n_k \times (J+1)$ matrix \mathbf{F}_{tk} consists of \mathbf{F}'_{it} 's and the $n_k \times n_k$ diagonal matrix $\boldsymbol{\Omega}_{tk}$ has ω_{itk} 's on the diagonal. This can be recognised as the joint distribution of the state vectors $\boldsymbol{\theta}_{tk}$ and observed data \mathbf{d}_{tk} for the Gaussian linear state space

model given by

$$\begin{aligned} \mathbf{d}_{tk} &= \mathbf{F}_{tk}\boldsymbol{\theta}_{tk} + \mathbf{v}_{tk}, & \mathbf{v}_{tk} &\sim N(\mathbf{0}, \boldsymbol{\Omega}_{tk}^{-1}), \\ \boldsymbol{\theta}_{tk} &= \boldsymbol{\theta}_{t-1,k} + \mathbf{e}_{tk}, & \mathbf{e}_{tk} &\sim N(\mathbf{0}, \boldsymbol{\Sigma}_{tk}), \end{aligned}$$

with the discount factor $\delta_{\boldsymbol{\Sigma}}$ for $\boldsymbol{\Sigma}_{tk}$. Then given the values for \mathbf{d}_{tk} , \mathbf{F}_{tk} , $\boldsymbol{\Omega}_{tk}$ and $\boldsymbol{\theta}_{1:T,k}$ can be sampled sequentially using the forward filtering and backward sampling (FFBS) described in the following. We introduce the common discount factor $\delta_{\boldsymbol{\Sigma}} \in (0, 1]$ for $\boldsymbol{\Sigma}_{tk}$.

- Forward filtering:

1. At the time $t - 1$, the posterior distribution of $\boldsymbol{\theta}_{t-1,k}$ is given by

$$\boldsymbol{\theta}_{tk} | \mathbf{d}_{1:t-1,k}, \mathbf{F}_{1:t-1,k} \sim N(\mathbf{m}_{t-1,k}, \mathbf{C}_{t-1,k}).$$

2. The prior distribution of $\boldsymbol{\theta}_{tk}$ at the time t is $\boldsymbol{\theta}_{tk} | \mathbf{d}_{1:t-1,k}, \mathbf{F}_{1:t-1,k} \sim N(\mathbf{a}_{tk}, \mathbf{R}_{tk})$, where $\mathbf{a}_{tk} = \mathbf{m}_{t-1,k}$, $\mathbf{R}_{tk} = \mathbf{C}_{t-1,k} / \delta_{\boldsymbol{\Sigma}}$.
3. The one-step ahead predictive distribution of \mathbf{d}_{tk} is given by $\mathbf{d}_{tk} | \mathbf{d}_{1:t-1,k}, \mathbf{F}_{1:t,k} \sim N(\mathbf{g}_t, \mathbf{Q}_t)$ where $\mathbf{g}_t = \mathbf{F}'_{tk} \mathbf{a}_{tk}$ and $\mathbf{Q}_{tk} = \mathbf{F}'_{tk} \mathbf{R}_{tk} \mathbf{F}_{tk} + \boldsymbol{\Omega}_{tk}^{-1}$.
4. The posterior distribution of $\boldsymbol{\theta}_{tk}$ at the time t is given by $\boldsymbol{\theta}_{tk} | \mathbf{d}_{1:t,k}, \mathbf{F}_{1:t,k} \sim N(\mathbf{m}_{tk}, \mathbf{C}_{tk})$ where $\mathbf{m}_{tk} = \mathbf{a}_{tk} + \mathbf{A}_{tk}(\mathbf{d}_{tk} - \mathbf{g}_{tk})$, $\mathbf{C}_{tk} = \mathbf{R}_{tk} - \mathbf{A}_{tk} \mathbf{Q}_{tk} \mathbf{A}'_{tk}$ and $\mathbf{A}_{tk} = \mathbf{R}_{tk} \mathbf{F}_{tk} \mathbf{Q}_{tk}^{-1}$.

- Backward sampling:

1. At the time T , sample from $\boldsymbol{\theta}_{Tk} | \mathbf{d}_{1:T,k}, \mathbf{F}_{1:T,k} \sim N(\mathbf{m}_{Tk}, \mathbf{C}_{Tk})$.
2. For $t = T - 1, T - 2, \dots, 1$, $\boldsymbol{\theta}_{tk}$ is sampled from the conditional distribution $\boldsymbol{\theta}_{tk} | \boldsymbol{\theta}_{t+1,k}, \mathbf{d}_{1:T,k}, \mathbf{F}_{1:T,k} \sim N(\mathbf{m}_{tk}^*, \mathbf{C}_{tk}^*)$ where $\mathbf{m}_{tk}^* = \mathbf{m}_{tk} + \delta_{\boldsymbol{\Sigma}}(\boldsymbol{\theta}_{t+1,k} - \mathbf{a}_{t+1,k})$ and $\mathbf{C}_{tk}^* = (1 - \delta_{\boldsymbol{\Sigma}})\mathbf{C}_{tk}$.

A.2 Sampling steps for MBPS2

The MCMC sampling proceeds in the same manner for MBPS2, but with some of the steps modified as the following and \mathbf{f}_{it} replaced with \mathbf{g}_{tk} with k such that $z_i = k$ in the rest of the steps.

Sampling z_i : The full conditional probability of $z_i = k$ is

$$P(z_i = k | \text{Rest}) \propto \pi_k \prod_{t=1}^T \left[\alpha(y_{it} | \mathbf{g}_{tk}, \boldsymbol{\theta}_{tk}) \prod_{j=1}^J h_{itj}(g_{tkj}) \right],$$

for $k = 1, \dots, K$.

Sampling \mathbf{g}_{tk} : We generate posterior samples of $\mathbf{g}_{tk} = (g_{tk1}, \dots, g_{tkJ})'$ rather than $\tilde{\mathbf{f}}_{it}$ from

$$p(\tilde{\mathbf{g}}_{tk} | \text{Rest}) \propto \prod_{i:z_i=k} \left[\alpha(y_{it} | \mathbf{g}_{tk}, \boldsymbol{\theta}_{tk}) \prod_{j=1}^J h_{itj}(g_{tkj}) \right].$$

By applying the Pólya-gamma augmentation, the full conditional distribution of \mathbf{g}_{tk} is $N(\hat{\mathbf{m}}_{tk}, \hat{\mathbf{S}}_{tk})$ where

$$\begin{aligned} \hat{\mathbf{m}}_{tk} &= \hat{\mathbf{S}}_{tk} \left[\sum_{i:z_i=k} \left(\left(\omega_{itk} (\log r - \theta_{tk0}) + \frac{y_{it} - r}{2} \right) \boldsymbol{\theta}_{-0,tk} + \mathbf{S}_{it}^{-1} \mathbf{m}_{it} \right) \right], \\ \hat{\mathbf{S}}_{tk} &= \left[\sum_{i:z_i=k} (\omega_{it} \boldsymbol{\theta}_{-0,tk} \boldsymbol{\theta}'_{-0,tk} + \mathbf{S}_{it}^{-1}) \right]^{-1}. \end{aligned}$$

A.3 Sampling steps for MBPS3

The sampling steps for MBPS3 is almost the same as those for MBPS1, but with some small modification due to the added term u_{it} .

Sampling $\boldsymbol{\theta}_{tk}$ and $\tilde{\mathbf{f}}_{it}$: The same sampling methods described above can be used, but now with the vector \mathbf{d}_{tk} being the collection of $(y_{it} - r)/2\omega_{itk} + \log r - u_{it}$.

Sampling u_{it} : For $i = 1, \dots, N$ and $t = 1, \dots, T$, the full conditional distribution of u_{it} is $N(\hat{u}_{it}, \hat{v}_{it}^2)$ where

$$\hat{u}_{it} = \hat{v}_{it}^2 \left(\omega_{itz_i} (\log r - \boldsymbol{\theta}'_{tz_i} \mathbf{F}_{it}) + \frac{y_{it} - r}{2} \right), \quad \hat{v}_{it}^2 = \left(\omega_{itz_i} + \frac{1}{\tau_{tk}^2} \right)^{-1}.$$

Sampling τ_{tk}^2 : The FFBS algorithm is used for the precision parameter $\varphi_{tk}^2 = 1/\tau_{tk}^2$ for $k = 1, \dots, K$.

- Forward filtering:

1. At the time $t-1$, the posterior distribution of $\varphi_{t-1,k}^2$ is given by the gamma distribution $Ga(a_{t-1}/2, b_{t-1}/2)$.
 2. The prior distribution at the time t is $Ga(\beta_\tau a_{t-1}/2, \beta_\tau b_{t-1}/2)$.
 3. At the time t , the posterior distribution is given by $Ga(a_t/2, b_t/2)$, where $a_t = \beta_\tau a_{t-1} + n_k$ and $b_t = \beta_\tau b_{t-1} + \sum_{i:z_i=k} u_{it}^2$.
- Backward sampling: If $t = T$, draw φ_{tk}^2 from $Ga(a_T/2, b_T/2)$, otherwise, $\phi_{tk}^2 = \varphi_{t+1,k}^2 + e_{tk}$ where $e_{tk} \sim Ga((1 - \beta_\tau)a_t/2, b_t/2)$, for $t = T - 1, \dots, 1$.

A.4 SIHR compartment model

The SIHR compartment model is given by the following system of differential equations:

$$dS/dt = -\alpha I \cdot S/N$$

$$dI/dt = \alpha I \cdot S/N - (\beta + \delta_I)I$$

$$dH/dt = \beta I - \delta_H H$$

$$dR/dt = \delta_I I + \delta_H H$$

where S , I , H and R are the numbers of susceptible, infected, hospitalised and recovered individuals, respectively, $\alpha, \beta, \delta_I, \delta_H \in (0, 1)$ are the parameters representing the infection rate, hospitalisation rate, recovering rate from the infected and hospitalised states, respectively. The Poisson means are modelled as the solution of the differential equations for H .

A.5 Coverages with the inflated variances

Table 3: Coverages of 95% prediction intervals for one-step-ahead prediction for Japanese and Korean data under the BPS models with the variances of the latent factors increased by five times

Country	s	MBPS1	MBPS2	MBPS3	BPS
Japan	1	0.559	0.368	0.929	0.582
Korea	1	0.910	0.284	0.969	0.936
	3	0.725	0.225	0.946	0.770
	7	0.639	0.248	0.949	0.696

A.6 Clustering results for Korean data

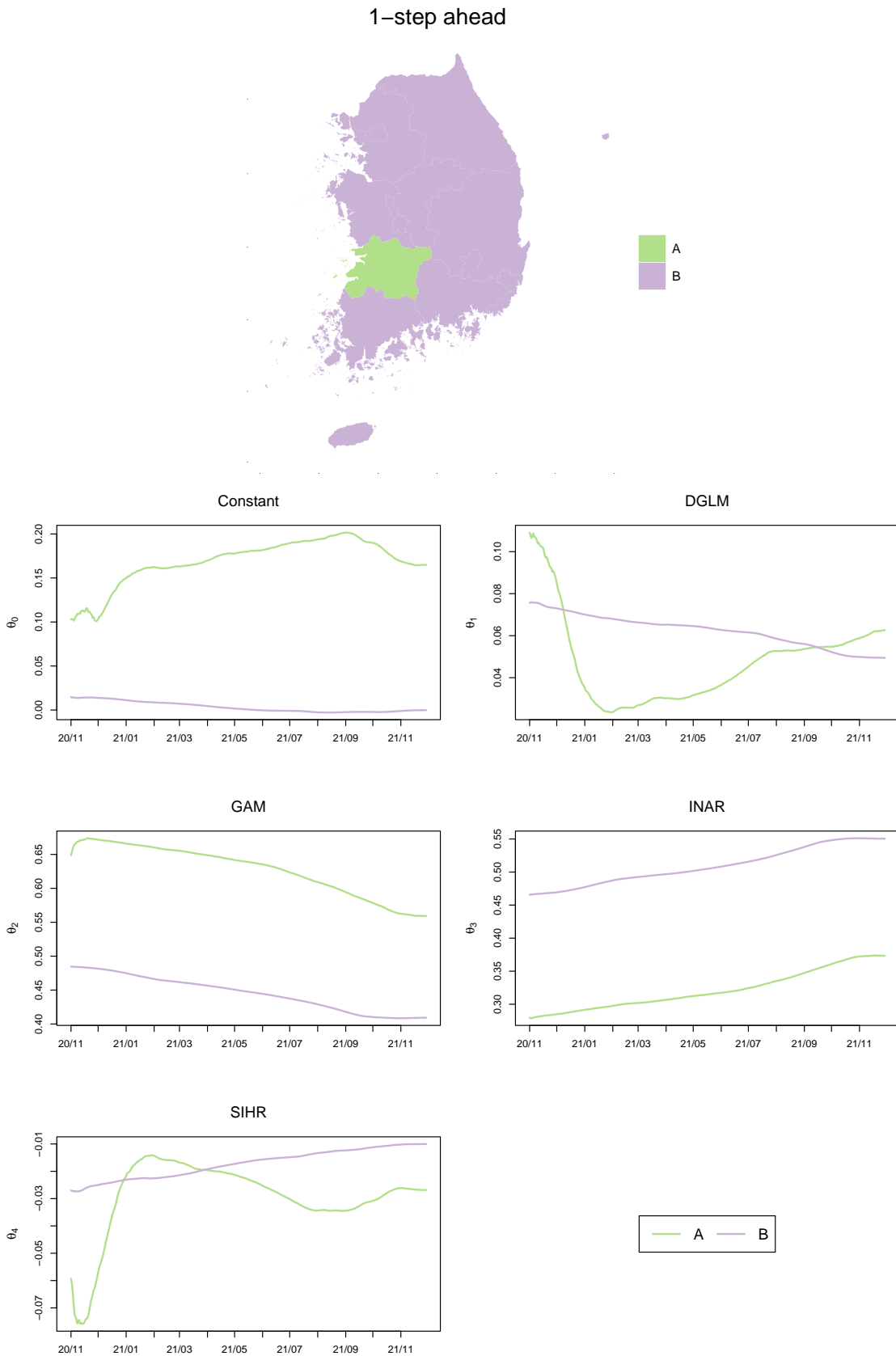


Figure 17: Clustered MAG (top maps) and posterior means of the synthesis weights under MBPS3 for one-step ahead prediction given all Korean data

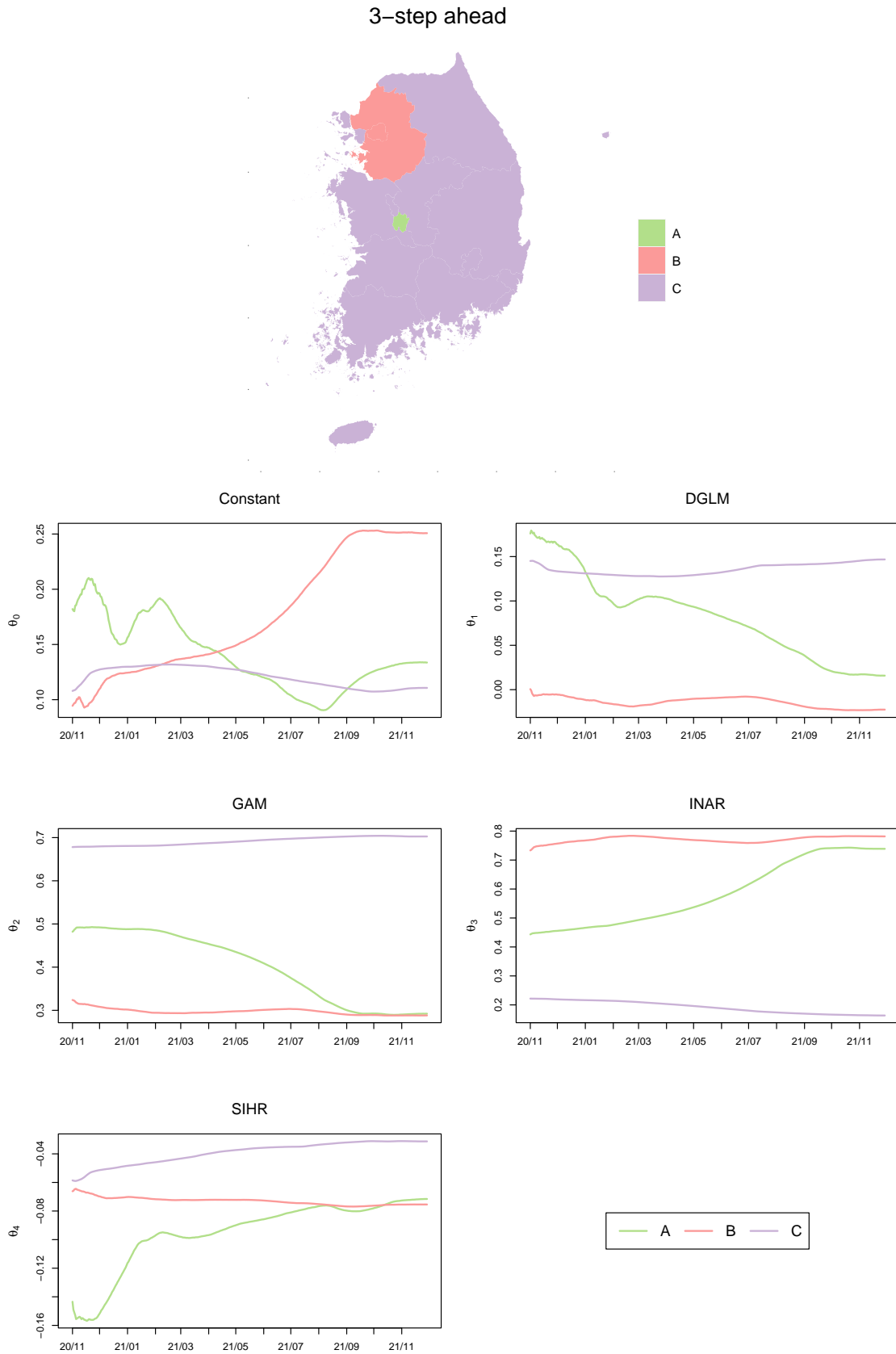


Figure 18: Clustered MAG (top maps) and posterior means of the synthesis weights under MBPS3 for three-step ahead prediction given all Korean data

References

- Aastveit, K. A., J. Mitchell, F. Ravazzolo, and H. K. van Dijk (2019). The evolution of forecast density combinations in economics. In *Oxford Research Encyclopedia of Economics and Finance*.
- Berry, L. R. and M. West (2020). Bayesian forecasting of many count-valued time series. *Journal of Business & Economic Statistics* 38(4), 872–887.
- Cabel, D., S. Shonosuke, M. Kato, K. Takanashi, and K. McAlinn (2023). Bayesian spatial predictive synthesis. *arXiv preprint arXiv:2203.05197*.
- Chernis, T. (2022). Combining large numbers of density predictions with bayesian predictive synthesis.
- Chowell, G., S. Dahal, A. Tariq, K. Roosa, J. M. Hyman, and R. Luo (2022). An ensemble n-sub-epidemic modeling framework for short-term forecasting epidemic trajectories: Application to the covid-19 pandemic in the usa. *PLoS Computational Biology* 18(10), e1010602.
- D’Angelo, L. and A. Canale (2022). Efficient posterior sampling for bayesian poisson regression. *Journal of Computational and Graphical Statistics* 0(0), 1–10.
- Davis, R. A., K. Fokianos, S. H. Holan, H. Joe, J. Livsey, R. Lund, V. Pipiras, and N. Ravishanker (2021). Count time series: A methodological review. *Journal of the American Statistical Association* 116(535), 1533–1547.
- Davis, R. A., S. H. Holan, R. Lund, and N. Ravishanker (Eds.) (2016). *Handbook of Discrete-Valued Time Series*. Chapman and Hall/CRC.
- Fisher, J. D., D. W. Puelz, and C. M. Carvalho (2020). Monotonic effects of characteristics on returns. *The Annals of Applied Statistics* 14(4), 1622 – 1650.
- Fokianos, K. (2021). Multivariate count time series modelling. *Econometrics and Statistics*.
- Frühwirth-Schnatter, S. (2011). Panel data analysis: a survey on model-based clustering of time series. *Advances in Data Analysis and Classification* 5(4), 251–280.

- Frühwirth-Schnatter, S. (1994). Data augmentation and dynamic linear models. *Journal of Time Series Analysis* 15(2), 183–202.
- Genest, C. and M. J. Schervish (1985). Modeling Expert Judgments for Bayesian Updating. *The Annals of Statistics* 13(3), 1198 – 1212.
- Hamura, Y., K. Irie., and S. Sugawara (2021). Robust hierarchical modeling of counts under zero-inflation and outliers. *arXiv preprint arXiv:2106.10503v1*.
- Johnson, M. C. and M. West (2023). Bayesian predictive synthesis with outcome-dependent pools. *arXiv preprint arXiv:1803.01984*.
- Lin, A., Y. Zhang, J. Heng, S. A. Allsop, K. M. Tye, P. E. Jacob, and D. Ba (2019). Clustering time series with nonlinear dynamics: A bayesian non-parametric and particle-based approach. In K. Chaudhuri and M. Sugiyama (Eds.), *Proceedings of the Twenty-Second International Conference on Artificial Intelligence and Statistics*, Volume 89 of *Proceedings of Machine Learning Research*, pp. 2476–2484. PMLR.
- McAlinn, K. (2021). Mixed-frequency bayesian predictive synthesis for economic nowcasting. *Journal of the Royal Statistical Society: Series C (Applied Statistics)*.
- McAlinn, K., K. A. Aastveit, J. Nakajima, and M. West (2020). Multivariate bayesian predictive synthesis in macroeconomic forecasting. *Journal of the American Statistical Association* 115, 1092–1110.
- McAlinn, K. and M. West (2019). Dynamic bayesian predictive synthesis in time series forecasting. *Journal of Econometrics* 210, 155–169.
- McCarthy, D. and S. T. Jensen (2016). Power-weighted densities for time series data. *The Annals of Applied Statistics* 10(1), 305 – 334.
- Nieto-Barajas, L. E. and A. Contreras-Cristán (2014). A Bayesian Nonparametric Approach for Time Series Clustering. *Bayesian Analysis* 9(1), 147 – 170.
- Paireau, J., A. Andronico, N. Hozé, M. Layan, P. Crépey, A. Roumagnac, M. Lavielle, P.-Y. Boëlle, and S. Cauchemez (2022). An ensemble model based on early predictors

- to forecast covid-19 health care demand in france. *Proceedings of the National Academy of Sciences* 119(18), e2103302119.
- Polson, N. G., J. G. Scott, and J. Windle (2013). Bayesian inference for logistic models using pólya–gamma latent variables. *Journal of the American statistical Association* 108(504), 1339–1349.
- Prado, R. and M. West (2010). *Time Series: Modeling, Computation, and Inference*. Chapman and Hall/CRC.
- Rahimi, I., F. Chen, and A. H. Gandomi (2023). A review on covid-19 forecasting models. *Neural Computing and Applications* 35(33), 23671–23681.
- Rousseau, J. and K. Mengersen (2011). Asymptotic behaviour of the posterior distribution in overfitted mixture models. *Journal of the Royal Statistical Society: Series B (Statistical Methodology)* 73(5), 689–710.
- Sugasawa, S., K. Takanashi, and K. McAlinn (2023). Bayesian causal synthesis for supra-inference on heterogenous treatment effects. *arXiv preprint arXiv:2304.07726*.
- Takanashi, K. and K. McAlinn (2023). Equivariant online predictions of non-stationary time series. *arXiv preprint arXiv:1911.08662*.
- Tallman, E. and M. West (2023). Bayesian predictive decision synthesis. *Journal of the Royal Statistical Society Series B: Statistical Methodology*, qkad109.
- West, M. (2020). Bayesian forecasting of multivariate time series: scalability, structure uncertainty and decisions. *Annals of the Institute of Statistical Mathematics* 72(1), 1–31.
- West, M. and J. Crosse (1992). Modelling probabilistic agent opinion. *Journal of the Royal Statistical Society: Series B (Methodological)* 54(1), 285–299.
- West, M. and P. J. Harrison (1997). *Bayesian Forecasting and Dynamic Models* (2nd ed.). Springer-Verlag.
- West, M., P. J. Harrison, and H. S. Migon (1985). Dynamic generalized linear models and bayesian forecasting. *Journal of the American Statistical Association* 80, 73–83.

Zhu, H.-T. and H. Zhang (2004). Hypthesis testing in mixture regression models. *Journal of the Royal Statistical Society: Series B (Statistical Methodology)* 66(1), 3 – 16.